

**THE CHARACTERISTICS AND ORIGIN OF COARSE LINEAR  
STRUCTURAL ELEMENTS IN PRECAMBRIAN GARNETIFEROUS  
BIOTITE SCHISTS AROUND SAWANTWADI, SINDHUDURG DISTRICT,  
SOUTHERN MAHARASHTRA.**

**A dissertation report for**

**GEO-651 Dissertation**

**Credits: 16**

**Submitted in partial fulfillment of Master's Degree**

**M.Sc. in Applied Geology**

**By**

**MELDROY VAS**

**Seat Number: 22P0450011**

**ABC ID: 414777307976**

**Under the supervision of**

**DR. NICOLE ANN FAE SEQUEIRA**

**School of Earth, Ocean and Atmospheric Sciences,**

**Applied Geology**



**GOA UNIVERSITY**  
गोय विद्यापीठ

**GOA UNIVERSITY**

**Date: APRIL 2024**



Examined by:

Seal of the School

## DECLARATION BY STUDENT

I hereby declare that the data presented in this Dissertation report entitled **The Characteristics and Origin of Coarse Linear Structural Elements in Precambrian Garnetiferous Biotite Schists around Sawantwadi, Sindhudurg District, Southern Maharashtra**. Is based on the results of investigations carried out by me in M.Sc. Applied Geology at the School of Earth, Ocean and Atmospheric Science, Goa University under the supervision of Dr. Nicole Sequeira and the same has not been submitted elsewhere for the award of a degree or diploma by me. Further, I understand that Goa University or its authorities will not be responsible for the correctness of observations / experimental or other findings given in the dissertation.

I hereby authorize the University authorities to upload this dissertation to the dissertation repository or anywhere else as the UGC regulations demand and make it available to anyone as needed.



Meldroy Vas

22P0450011

Date: 02/05/2024  
Place: Goa University

## COMPLETION CERTIFICATE

This is to certify that the dissertation report '**The Characteristics and Origin of Coarse Linear Structural Elements in Precambrian Garnetiferous Biotite Schists around Sawantwadi, Sindhudurg District, Southern Maharashtra**' is a bonafide work carried out by Mr. Meldroy Vas under my supervision in partial fulfillment of the requirements for the award of the degree of M.Sc. in the Discipline Applied Geology at the School of Earth, Ocean and Atmospheric Science, Goa University.

Date: 02.05.2024



Dr. Nicole Sequeira  
Assistant professor  
Goa University



Senior Prof. Sanjeev Ghadi  
Dean  
Goa University  
School of Earth, Ocean and Atmospheric Science

Date:

Place: Goa University



School Stamp

**THE CHARACTERISTICS AND ORIGIN OF COARSE LINEAR  
STRUCTURAL ELEMENTS IN PRECAMBRIAN GARNETIFEROUS  
BIOTITE SCHISTS AROUND SAWANTWADI, SINDHUDURG DISTRICT,  
SOUTHERN MAHARASHTRA.**

**A dissertation report for**

**GEO-651 Dissertation**

**Credits: 16**

**Submitted in partial fulfillment of Master's Degree**

**M.Sc. in Applied Geology**

**By**

**MELDROY VAS**

**Seat Number: 22P0450011**

**ABC ID: 414777307976**

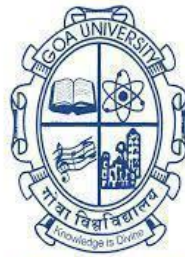
**PRN: 201902312**

**Under the supervision of**

**DR. NICOLE ANN FAE SEQUEIRA**

**School of Earth, Ocean and Atmospheric Sciences,**

**Applied Geology**



**GOA UNIVERSITY**  
गोंय विद्यापीठ

**GOA UNIVERSITY**

**Date: MAY 2024**

**THE CHARACTERISTICS AND ORIGIN OF COARSE LINEAR  
STRUCTURAL ELEMENTS IN PRECAMBRIAN GARNETIFEROUS  
BIOTITE SCHISTS AROUND SAWANTWADI, SINDHUDURG DISTRICT,  
SOUTHERN MAHARASHTRA.**

**A dissertation report for**

**GEO-651 Dissertation**

**Credits: 16**

**Submitted in partial fulfillment of Master's Degree**

**M.Sc. in Applied Geology**

**By**

**MELDROY VAS**

**Seat Number: 22P0450011**

**ABC ID: 414777307976**

**Under the supervision of**

**DR. NICOLE ANN FAE SEQUEIRA**

**School of Earth, Ocean and Atmospheric Sciences,  
Applied Geology**



**GOA UNIVERSITY**

**Date: APRIL 2024**

Examined by:

Seal of the School

## **DECLARATION BY STUDENT**

I hereby declare that the data presented in this Dissertation report entitled **The Characteristics and Origin of Coarse Linear Structural Elements in Precambrian Garnetiferous Biotite Schists around Sawantwadi, Sindhudurg District, Southern Maharashtra**. Is based on the results of investigations carried out by me in M.Sc. Applied Geology at the School of Earth, Ocean and Atmospheric Science, Goa University under the supervision of Dr. Nicole Sequeira and the same has not been submitted elsewhere for the award of a degree or diploma by me. Further, I understand that Goa University or its authorities will not be responsible for the correctness of observations / experimental or other findings given in the dissertation.

I hereby authorize the University authorities to upload this dissertation to the dissertation repository or anywhere else as the UGC regulations demand and make it available to anyone as needed.

Meldroy Vas

22P0450011

Date:

Place: Goa University

## **COMPLETION CERTIFICATE**

This is to certify that the dissertation report '**The Characteristics and Origin of Coarse Linear Structural Elements in Precambrian Garnetiferous Biotite Schists around Sawantwadi, Sindhudurg District, Southern Maharashtra**' is a bonafide work carried out by Mr. Meldroy Vas under my supervision in partial fulfillment of the requirements for the award of the degree of M.Sc. in the Discipline Applied Geology at the School of Earth, Ocean and Atmospheric Science, Goa University.

Date:

Dr. Nicole Sequeira  
Assistant professor  
Goa University

Senior Prof. Sanjeev Ghadi  
Dean  
Goa University  
School of Earth, Ocean and Atmospheric Science

School Stamp

Date:

Place: Goa University

## **ACKNOWLEDGEMENT**

Firstly, I would like to express my immense gratitude to my guide, Dr. Nicole Sequeira, Applied Geology, School of Earth, Ocean and Atmospheric Sciences, for her invaluable guidance, support and untiring effort during the course of my dissertation. She has been a great source of motivation and encouragement for me to undertake this topic as my study.

I am also grateful to Sr. Prof. Sanjeev C. Ghadi, Dean, and Dr. Anthony A. A. Viegas, Vice Dean, School of Earth, Ocean and Atmospheric Sciences, and the faculties of Applied Geology, Dr. Niyati Kalangutkar, Mr. Mahesh Mayekar, and Dr. Pooja Ghadi, for their willingness to assist me whenever approached.

I extend my sincere thanks to Mr. Rajesh Mangeshkar, Mrs. Sangeeta Tilve, Mrs. Tulsi, and all other non-teaching and laboratory staff members. I would also like to thank my senior, Mr. Pratik Santra and Jane Pereira for their help during the dissertation work.

I am grateful to my parents, my siblings, and my friends Liana Fernandes, Juyee Priolkar, Yadhanesh Vazarkar, Meldrin Afonso, Sakshi Parwar, Simran Shecar, Deevyam Rawal and Becca Rodrigues for their encouragement and moral support throughout the course of the dissertation.

## **Table of Contents**

CHAPTER 1- INTRODUCTION.....	1
INTRODUCTION.....	2
AIMS & OBJECTIVES .....	5
STUDY AREA.....	5
PHISIOGRAPHY .....	6
METHODOLOGY .....	6
CHAPTER II- LITERATURE REVIEW .....	8
GEOLOGY OF DHARWAR CRATON .....	9
GEOLOGY OF THE STUDY AREA .....	14
CHAPTER III - FIELD CHARACTERISTICS AND STRUCTURAL ANALYSIS .....	17
FIELD CHARACTERISTICS AND STRUCTURAL ANALYSIS. ....	19
CHAPTER IV- PETROGRAPHIC ANALYSIS.....	30
PETROGRAPHY AND MINERAL CHEMISTRY .....	31
CHAPTER V- GEOTHERMOBAROMETRY.....	31
GEOTHERMOBAROMETRY.....	45
CHAPTER VI- DISCUSSION & CONCLUSION .....	48
DISCUSSION & CONCLUSION .....	49
REFERENCES.....	53

## LIST OF FIGURES

Figure No	Title of Figures	Page No
Fig 1	Marked and labeled diagram of a sheath fold modified after (Alsop & Holdsworth (2006)).	2
Fig 2	Detailed geological map of Dharwar Craton.	10
Fig 3	Generalized geological map of Pernem-Phonda corridor from Rekha and Bhattacharya (2014).	13
Fig 4	Map of study area with rose diagrams of attitudes of sheath folds and foliation data.	18
Fig 5- 14	Field photographs.	21-24
Fig. 15	Stereographic projections of planes and rose diagrams.	25
Fig 16	Stereographic projections of Poles and Plunges.	26
Fig 17	Data on coarse lineations showing variation in plunges	27
Fig 18	Strike and dip of the coarse lineations defining an intrafolial fold in the E-W foliation	27
Fig 19	Elliptical ratio-Ryz of coarse lineations.	28
Fig 20	Ryz ratios of Coarse Lineations near hinge of the fold and at the limbs of the fold.	28
Fig 21	Photomicrograph of Coarse Lineation under Plane Polarized light with different layers and figure number of cropped images marked.	35
Fig 21	Detailed images of textures and microstructures	35-37
Fig 22	Feldspar anorthite, orthoclase, and albite ternary diagram with compositional subdivisions.	38
Fig 23	Plot of Ca±Mg±Fe pyroxene data on ternary classification diagrams with distinguished pyroxene names	38
Fig 24	Classification diagram for matrix and Layer 3 garnets.	39
Fig 25	Compositional plot of biotite in the phlogopite–annite–siderophyllite–eastonite system.	39
Fig 26	Al, Ca, Fe, Na and Si X-ray element maps of the sheath fold.	40
Fig 27	Formation of sheath fold around a competent layer modified after Marques et al, (2008).	45

## LIST OF TABLES

<b>Table No</b>	<b>Title</b>	<b>Page No</b>
Table 1	Electron Probe micro analytical data and structural formula for pyroxene on the basis of 6 oxygen.	41
Table 2	Electron Probe micro analytical data and structural formulae for Garnets. On the basis of 12 oxygen.	41
Table 3	Electron Probe micro analytical data and structural formulae for feldspars on the basis of 8 oxygen.	42
Table 4	Electron Probe micro analytical data and structural formulae for biotites. On the basis of 11 oxygen	42
Table 5	Geothermometry of the sheath fold and matrix at 7.5kbar pressure.	45
Table 6	Geobarometry of sheath folds and matrix at temperature 600°C.	46

## ABSTRACT

The study focuses on the characteristics and origin of the variably plunging coarse lineation structures in the Precambrian garnetiferous biotite schists in the NW of Sawantwadi town, Sindhudurg district, Maharashtra, India. Detailed structural field observations indicate that the lineations earlier reported as sheath folds are elliptical in cross-section, multilayered with pink cores and have variable plunges. In high strain domains, they are parallel to the successive N-S, E-W, NW and ENE foliation in the schists but they are observed to define intrafolial folds to the E-W foliation in the low-strain domains. Petrographic analysis indicates that the lineations have concentric layers with varying mineralogy: From core to rim, Layer 1: Hornblende + plagioclase + quartz. Layer 2: diopside (with hornblende coronas) + quartz + plagioclase. Layer 3: garnet + diopside + epidote + calcite + titanite. EPMA analysis of the silicate minerals in the individual layers indicate that XCa in plagioclase decreases from core to rim, clinopyroxene composition varied between 38-65% XFe in the Layers 2 and 3 and garnets in the core are Ca-Fe rich but Fe-Mn-Mg rich in the matrix. Biotite is homogenous in the matrix. Grt-cpx, grt-hbl, biotite-garnet geothermometers and hbl-plag geobarometers using minerals from individual layers indicate that the temperature and pressure during the formation of these linear structures were 620-625°C for layer 1 & layer 2 and increases to 685°C in the core at pressure 7.5kbars. Combining the different datasets it is concluded that the linear structures are rods that have developed from interbanded calc-silicate layers in the biotite schist, and not sheath folds. The rodding possibly initiated during the N-S foliation formation but also progressed during the later deformations. This indicates that rheologic differences in protoliths control the formation of linear stretching structures developed within progressively deformed amphibolite facies metamorphic schists.

## **CHAPTER 1**

### **INTRODUCTION**

## INTRODUCTION

Lineations are elongated structural features within rocks that offer valuable insights into a rock's history (e.g., stretching due to shearing forces [Hobbs et al., 2006]). These linear structures, like stripes or streaks, can arise from various geological processes, including folding, faulting, or shearing (Twiss & Moores, 1992). By studying the type, orientation, and intensity of lineations, we can reconstruct the forces that deformed the rocks and determine the direction of those forces (Jones & Lister, 1990). There are several distinct types of lineation: stretching lineation (elongated minerals parallel to shearing), mineral lineation (preferred orientation of elongated minerals), intersection lineation (formed by intersecting planar features like bedding and foliation), and crenulation lineation (folds in pre-existing foliation) (Fossen, 2016).

Two types of coarse lineations, sheath folds and rods, can sometimes be confused due to their similar appearances in field. A sheath fold is a type of coarse stretching lineation formed along the slip surface of a shear plane and a rod is a type of coarse stretching lineation formed due to layer parallel stretching of multilayered rocks with high competency contrasts.

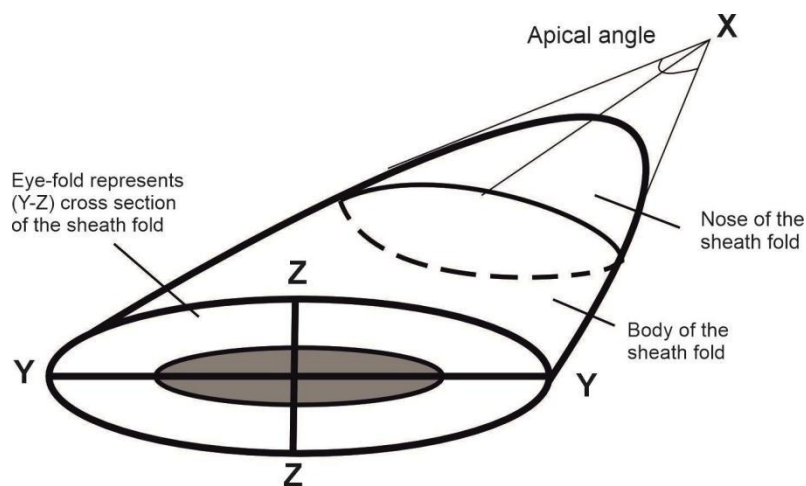


**Fig 1:** Schematic diagram of a sheath fold modified after Alsop & Holdsworth (2006)

Sheath folds are highly non-cylindrical structures that are frequently connected to shear zones (e.g., Carreras et al., 1977). Non-cylindrical folds are categorized as sheath folds by Ramsay and Huber (1987) when the angle at which their cone opens is less than 90. Because they are thought to provide information on strain magnitude (e.g., Minnigh, 1979), bulk strain type (Alsop and Holdsworth, 2006), and shear direction (Fossen and Rykkelid, 1990), they are of interest to field geologists. Besides field investigations, laboratory (e.g., Cobbold and Quinquis, 1980; Rosas et al., 2002; Marques et al., 2008; Reber et al., 2013), numerical (e.g., Mandal et al., 2009; Vollmer, 1988), and analytical (Reber et al., 2012) models are used to study their formation mechanisms. There have been several proposed methods for how sheath folds arise. They can either arise by constriction and flattening (such as in Ez, 2000; Mandal et al., 2009; Nicolas and Boudier, 1975) or simple shear (such as in Carreras et al., 1977; Fossen and Rykkelid, 1990; Minnigh, 1979).

Even though sheath folds are three-dimensional structures, they are commonly observed in the field on two-dimensional crosssections. Cross-sections perpendicular to the elongation direction of the cone exhibit strongly deformed layers and closed contours, which can be described as “eyes”. Sheath folds can be described as containing an x axis along the length of the tube or tongue, whilst cross sections normal to the x axis display elliptical geometries defining the intermediate (y) and short (z) axes. The distinctive feature of sheath folds is their appearance, resembling a stack of cylindrical layers that wrap around a central core. This core is usually composed of more resistant rock layers, which can withstand the folding process, while the surrounding layers fold and wrap around it.

Rodding is a process by which pre-existing layered rock formations undergo a remarkable transformation. These layered units are stretched and sculpted by immense

directed stress during various deformation events, ultimately morphing into elongated, cylindrical structures known as rods (Fossen, 2016). These rod-shaped features preserve a record of the strain history endured by the rock mass.

The driving force behind rodding lies in the concept of high strain, encompassing extreme stretching, shortening, or shearing forces acting upon the rock (Twiss & Moores, 1992). The competency variations within the layered unit play a critical role. The competent layers possess superior resistance to deformation compared to the surrounding incompetent layers. Due to this inherent strength difference, competent layers are much more susceptible to rodding (Ramsay & Lisle, 2000). During deformation, these competent layers experience preferential stretching and attenuation in the direction of the dominant principal stress, essentially being squeezed and elongated into rod-like structures. Conversely, the incompetent layers, due to their weaker mechanical properties, tend to flow or become pinched and boudinaged between the competent layers (Ghosh, 2004).

Rodding is a crucial tool in structural geology as it provides valuable insights into the deformation history of a rock mass. Shear direction can be determined by noting the orientation of the rodding axis, defined by the alignment of elongated minerals or clasts, directly reflecting on the direction of the shearing forces that deformed the rock (Simpson & Schmid, 1983). Strain intensity can be determined by the degree of rodding development and can be indicative of the intensity of shearing. Highly sheared rocks often exhibit strong rodding development, with extreme elongation and alignment of competent minerals (Berthé et al., 2001). The specific type and orientation of rodding can vary depending on the local shearing conditions (e.g., temperature, pressure, strain rate) (Rosenfeld et al., 1998). This variation allows us to differentiate between different

shear zones within an area and reconstruct the overall deformation history. By studying shear structures like foliation, sheath folds, veins and rodding we can gain a comprehensive understanding of the complex forces that shaped the rocks in any area chosen for investigation.

### **AIMS & OBJECTIVES**

The work is aimed at understanding the structural evolution of the coarse linear structures in the Precambrian garnetiferous biotite schists NW of Sawantwadi, Sindhudurg district, Maharashtra, through detailed structural field mapping, petrographic analysis and geothermobarometry.

1. To identify the extent, structural variations and strain patterns of the coarse linear structural elements in the study area.
2. To characterize the mineralogy, microstructure and mineral chemistry of the phases within the linear structural elements
3. To infer the origin of the linear structural elements and their relationships with the regional tectonic deformation.

### **STUDY AREA**

The study area is situated on the west coast of India in the Sindhudurg district of Maharashtra. The study area delineated by the coordinates N 15°51'-N16°04' and E 73°49'-E73°50', is bordered by the villages of Madhkol to the west, Ghotos to the north, Kesari to the south, and Vasoli to the east. Nearby towns such as Kudal, Sawantwadi, and Kankavali are accessible via National Highway (NH-17), linking to Panaji, Pune, and Kolhapur. Challenges in road accessibility are prominent along the

southeastern, eastern, and northeastern sides, which are mountainous and part of the ghat region. The toposheet numbers of the study area are 47H/16/SE and 48E/13.

## **PHYSIOGRAPHY**

Sindhudurg district is located in Maharashtra's Konkan region and covers 5207 square kilometers. The district is on Survey of India degree sheets 47H, 48 E, and 48 I. The district is situated between East longitude 73° 19' and 74" 13 and north latitude 15°37" and 16" 40'. The district has a geographical area of 5207 square kilometers, of which 386.43 square kilometers are covered by forest, while 3222 square kilometers are cultivable. Sown area net is 1522 square kilometers. Sawantwadi and Kankavli are the district's two revenue sub-divisions. Sawantwadi, Vengurla, Kudal, Kankavli, Malvan, Deogad, Dodamarg and Vaibhavwadi are the district's eight talukas. The district is bounded by Ratnagiri district to the north and the Arabian Sea to the west, Kolhapur district is located to the east and Goa State and the Belgaum district of Karnataka State are to the south. The Western Ghats run through the district, providing a natural boundary between the district and the rest of Maharashtra. The district consists primarily of hilly terrain, with an average elevation of 600-800 meters above sea level. The district's highest point is Ramtirth, which is approximately 900 meters above sea level.

## **METHODOLOGY**

The region including Sawantwadi and Kudal was selected, and Google Earth was utilized to create a route map. Locations were selected from satellite imagery because the chosen area is rugged, mountainous, and covered in dense forest. The sites were identified using a GPS. The lithological map of the area was digitized from the existing

maps released in GSI reports (GSI open file report Maharashtra, 2018). From May 2023 to February 2024, fieldwork and systematic sampling were conducted. Numerous structural features, including foliation, folds, and quartz veins, were noticed during fieldwork. The strike and dip data of the structures were measured using a Clinometer compass and noted in the field notebook. Sketches of the features in the rocks were made on the field notebook and field photographs were taken using appropriate scale. Care was taken to orient the scale in the N-S direction. The location map of the area with structural data was then made. Stereographic projections and Rose diagrams were created by using GEORient software (version 9.5.0). Thin sections for micro-fabric examination were prepared after samples were cut into chips perpendicular to the foliation and parallel to the lineation. The Nikon Eclipse E 200 microscope was used to examine the thin sections. Mineral chemical data of the silicate minerals in the thin sections was obtained from the National facility housing the Electron Probe Micro Analyzer (EPMA) at the Department of Earth Sciences, IIT Bombay, Mumbai, India. Application PTQuick and Excel sheet 'GARNET-BIOTITE THERMOMETER - Seven calibrations' was used to do thermobarometric calculations. The different data sets were then integrated to understand the characteristics and origin of the coarse linear structural elements in the study area.

## **CHAPTER II**

### **LITERATURE REVIEW**

## **GEOLOGY OF DHARWAR CRATON**

Precambrian rocks make up the majority of Peninsular India, which is separated into six distinct crustal regions: the Dharwar craton, the Eastern Ghats, the Bastar-Bhandara, Singhbhum, and Bundelkhand cratons, and the Southern Granulite terrain that adjoins them. The Dharwar craton is covered by the Cuddapah basin in the northeast, the Southern Granulite terrain in the south, and the Deccan traps in the northwest. The Bastar and Dharwar cratons are divided by the Pranhita Godavari basin. On both sides of the basin are the Granulites. The Dharwar craton and the Southern Granulite terrain are divided by the Palghat Cauvery Shear Zone. It is believed that the Dharwar craton rises to the Central Indian Tectonic Zone and is the basement of the Deccan Traps.

The Dharwar Craton, situated in southern India, exposes the oldest continental crust on the Indian peninsula, with formation spanning the Archean eon (3.6-2.5 billion years ago). Geological investigations reveal a complex evolutionary history characterized by distinct terranes (tectonic blocks) sutured together over time. The basement complex, primarily composed of TTG gneisses (Tonalite-Trondhjemite-Granodiorite), crystallized around 3.0 Ga. This formation is attributed to a combination of intraplate hotspot activity, subduction-related magmatism from a downgoing oceanic slab, and arc magmatism from a thickened oceanic arc complex. Recent studies delineate the craton into three distinct terranes: the Western Dharwar Craton (WDC), Central Dharwar Craton (CDC), and Eastern Dharwar Craton (EDC). (V Rao et al. 2021).

The western Dharwar Craton boasts the oldest record, evidenced by extensively metamorphosed greenstone sequences (schists) formed through submarine sedimentation and volcanic eruptions between 3.0 and 3.4 Ga. These sequences offer invaluable insights into the Earth's early history. (Mishra et al. 2013).

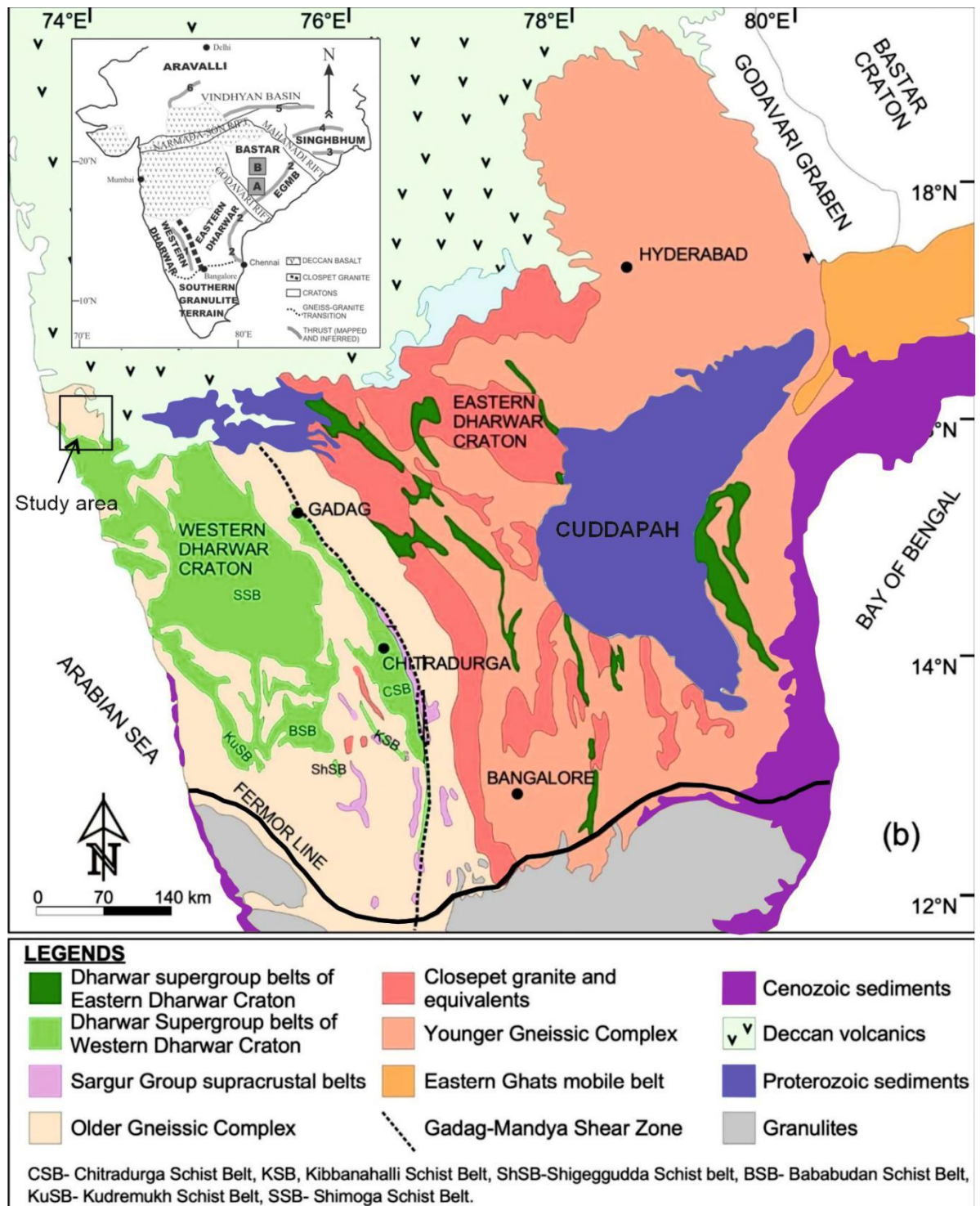


**Fig 2:** Detailed geological map of Dharwar Craton with Fig 3 area marked. Modified after ( L.sreehari et al. 2020).

The Central Dharwar Craton is dominated by migmatitic TTG gneisses formed around 3.0 Ga. Migmatization signifies a period of intense heat and pressure that caused granitic melts to intrude and partially melt the existing gneisses, resulting in a complex

and distinctive rock assemblage. This terrane likely represents a period of relative stability within the craton's evolution (V. Rao et al. 2021).

The Eastern Dharwar Craton presents a contrasting picture with younger greenstone belts and calc-alkaline plutons, crystallized at approximately 2.7 Ga. This significant age difference and distinct lithology suggest a unique geological history compared to the other terranes. It's hypothesized that separate accretionary events amalgamated these blocks to form the present-day Dharwar Craton (Ramakrishnan, M & Vaidyanathan, S. 2008).

The two groups in the volcano-sedimentary greenstone sequences are the Older Sargur Group (3.1-3.3 Ga) and the younger Dharwar Supergroup (2.6-2.8 Ga) (Hokada, 2013). The Sargur Group is dominated by komatiitic to high Mg basaltic volcanic rocks, subordinate basaltic to felsic rocks and interlayered shallow shelf assemblages. And it can be found as either linear mafic-ultramafic belts that progressively narrow or as clusters of enclaves strewn across the craton (Ramakrishnan and Vishwanatha, 1981; Jayananda et al., 2008;). The Dharwar Supergroup in the WDC is further divided into the lower Bababudan Group and the upper Chitradurga Group (Ramakrishnan and Vaidyanadhan., 2010). The Bababudan group contains low grade Volcano-sedimentary sequences with an unconformable contact with the supracrustal rocks and the basement. Conglomerates and quartzites are attributed to fluvial environments where quartzite shows cross bedding and the environment is inferred as shallow- water environment. Upper Chitradurga group is begins with oligomictic conglomerate followed by basaltic flows, greywacke-argillite, carbonaceous phyllites, intermediate to felsic volcanics (pyroclastic) and thick banded iron formations. The oligomictic conglomerate-quartzite-carbonate are inferred as deposited in shallow water sequences in the SW and

the greywacke-argillite-carbonaceous shale-BIFs were in progressively deep-water facies in NE (Swami Nath and Ramakrishnan, 1981).

In the EDC, it comprises the schist belts of Kolar, Kadiri, Raichur and Hutti belts. These schist belts are important in the aspect of gold mineralization. The Block is dominated by volcanic rocks including minor ultramafics and sedimentary sequences (Ramakrishnan and Vaidyanadhan, 2010).

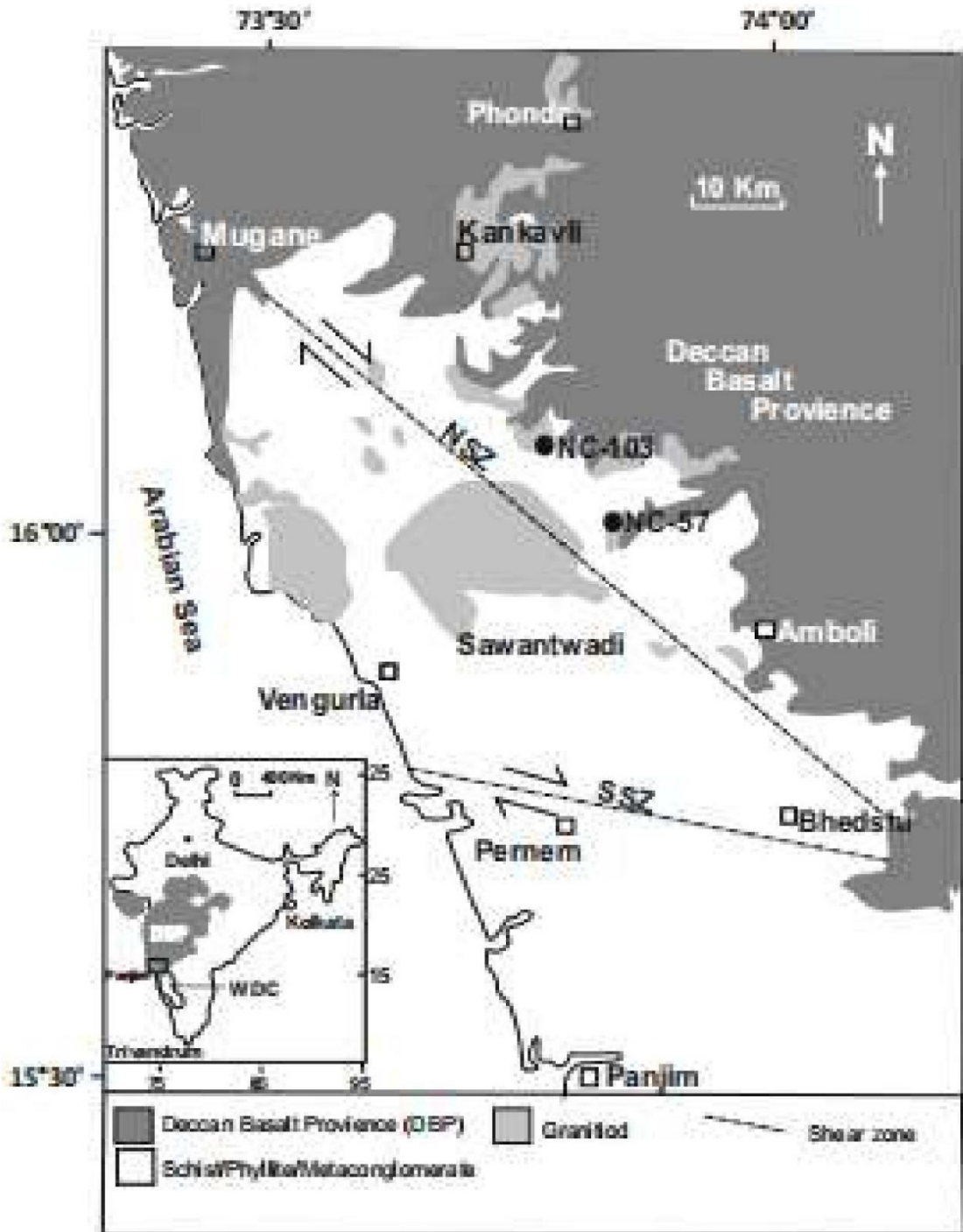


**Fig 3:** Generalized geological map of Pernem (Goa)-Phonda (Maharashtra) corridor from Rekha and Bhattacharya (2014).

## **GEOLOGY OF THE STUDY AREA**

Situated within the Konkan region, between the Arabian Sea and the Western Ghats, Sindhudurg district boasts a diverse geological landscape. Initially classified as the “Older Metamorphic Series” by Wilkinson in 1871, these rocks were later grouped by Foote in 1876 into the Gneissic Series and Dharwar System. Iyer (1939) further categorized the pre-trappean rocks of South Konkan and Maharashtra under the Metamorphic and Unmetamorphosed Kaladgi Series. Kelkar (1956) identified two main groups of Archean metamorphic rocks, distinguished by a thrust contact between them. Group I includes granite gneiss, quartzites, mica schists (garnet), staurolite and kyanite, biotite, and hornblende granulites, while Group II consists of coastal rocks like crushed conglomerate, phyllites, and ferruginous quartzites. Ghodke (1983) classified the metamorphic rocks of Sindhudurg as part of the Banda Group, suggesting their equivalence to the middle and upper divisions of the Dharwar Supergroup. Additionally, Naqvi & Rogers (1987) noted the presence of schists along the Western coast of India and Goa, possibly extending northward into Karwar. However, studies primarily focused on the northwest, west, and far south of the district, with few attempts made to establish the interrelationship between the supracrustal rocks of these areas. The lithology of the region is characterized by a sequence of metagreywackes and amphibolites intruded by various generations of granitoids, interspersed with banded iron formations (BIF) and quartzites. The southern part of the district forms the northwestern section of the highly deformed and evolved Dharwar Craton, where supracrustal rocks exhibit superimposed deformation (Deshpande; Pitale 2014; Rekha and Bhattacharya 2014).

Rekha and Bhattacharya (2014) recently identified two distinct shear zones within the Study area NNW-trending Northern Shear Zone (NSZ) characterized by gently

dipping foliation and open folds with NW-trending axial planes, and a WNW-trending Southern Shear Zone (SSZ) featuring subvertical to steeply south dipping foliations and reclined folds with WNW-trending axial planes. The rocks in the study area have been dated as Precambrian crystalline rocks through Th-U-Pb chemical monazite geochronology. South of the SSZ, ages of the Goa Schist Belt range between 2.4 and 2.6 billion years (Ga), with a statistical peak of  $2520 \pm 18$  million years (Ma) and a subsidiary Paleoproterozoic age population of  $2366 \pm 21$  Ma. Additionally, the metamorphic age of greenschist facies supracrustal rocks in the Goa Schist Belt of the Western Dharwar Craton (WDC) has been estimated to be approximately 2.5 Ga. In the schists between the SSZ and the NSZ, the dominant statistically resolved ages in monazites are Paleoproterozoic ( $2385 \pm 14$  Ma,  $2192 \pm 17$  Ma, and  $1872 \pm 14$  Ma), with a minor population of Mesoproterozoic ages ( $\sim 1460$  Ma). Notably, the 2.5-2.6 Ga age in the greenschist facies supracrustal rocks of the Goa Schist Belt south of the SSZ is uncommon in samples north of the SSZ. The lithologies north of the NSZ exhibit Paleoproterozoic ages ( $2303 \pm 12$  Ma,  $2198 \pm 15$  Ma,  $2088 \pm 16$  Ma,  $1953 \pm 22$  Ma, and  $1788 \pm 27$  Ma), consistent with those observed between the SSZ and NSZ. The prominent Mesoproterozoic mean age ( $1673 \pm 15$  Ma) in this region is attributed to spot ages obtained from quartzite.

Sheath folds were earlier reported in this area by Rekha and Bhattacharya (2014), the axes of these folds are distributed along the mean orientation of the shear zone fabric, and the folds get tighter with curved hinge lines. These folds general ellipsoidal geometry is comparable to the superposition structure of basin and dome folds. (C.F. Kelly et al. 2000) But since the fold hinges at the margin of the ellipsoidal folds are parallel to the long axes of these folds, and the folds are not symmetrically disposed as in dome-basin structures, it was inferred that the ellipsoidal folds to be immature

sheath fold formed due to single deformation. (Cobbold and Quinquis, 1980) (Ghosh et al. 1999). The presences of sheath folds in the study area has also been mentioned by (Azhar. C, 2022) and (Venugopal, 2023).

## **CHAPTER III**

### **FIELD CHARACTERISTICS AND STRUCTURAL ANALYSIS.**

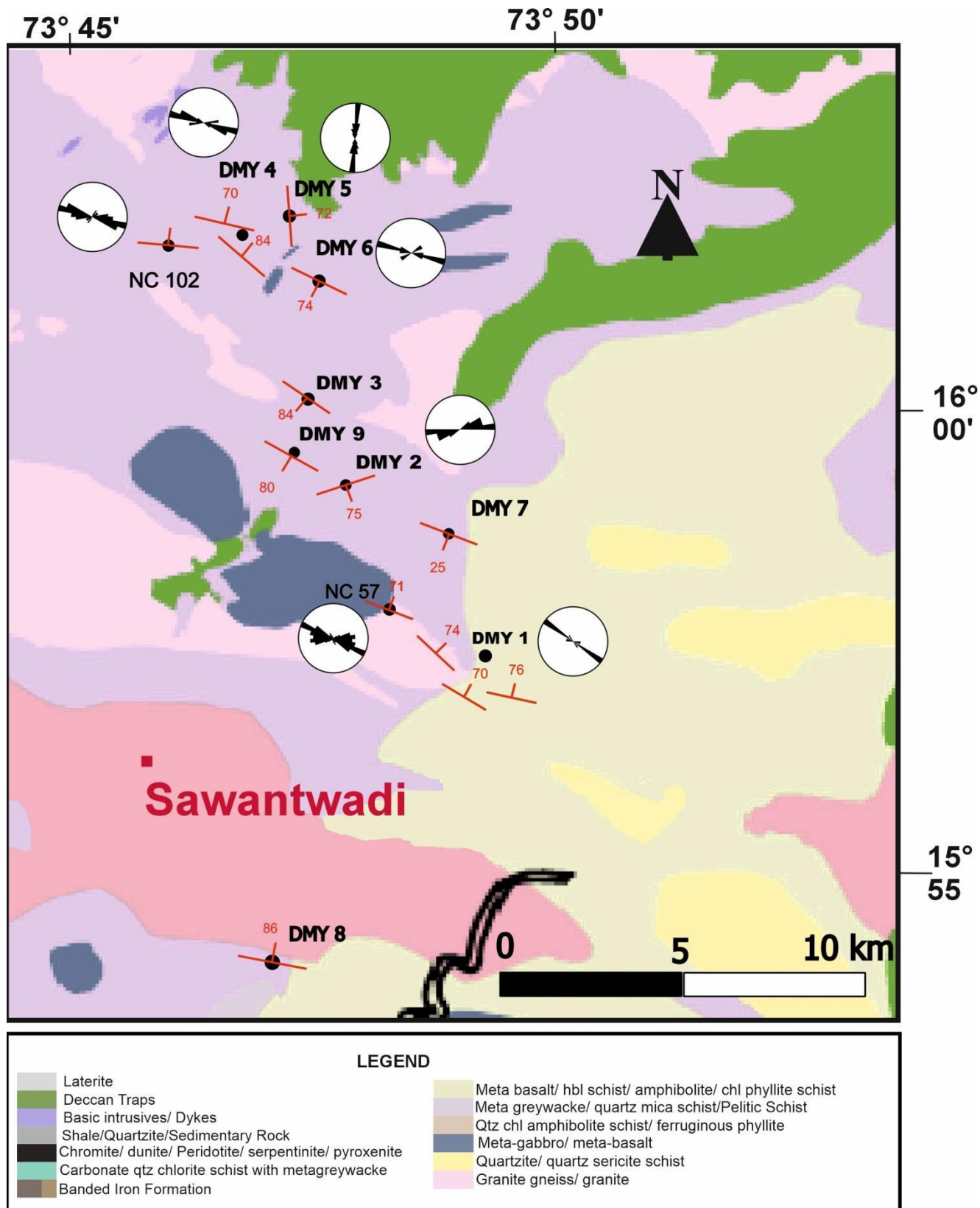


**Fig 4:** Lithological map of study area modified from GSI District map (2021) The penetrative foliation data at the selected locations are shown in red. Rose diagrams compiled from Y axes orientations of coarse linear structural elements from each location are shown beside the location numbers

## **FIELD CHARACTERISTICS AND STRUCTURAL ANALYSIS.**

The study area consists of Precambrian garnet mica schists interlayered with 10s of cm thick continuous and discontinuous calc-silicate bands. The garnets in the schists are millimeters in size and can be identified through the unaided eye and is dispersed throughout the rock. The garnet porphyroblasts are pinkish to reddish brown, with a euhedral shape. The schists are generally fine grained and the orientation of foliation planes are sometimes difficult to identify in these dark coloured country rocks. The garnet mica schist have undergone multiple generations of deformation producing several sets of penetrative foliations in the area.

The foliations identified in the study area are:

1. Shallow dipping foliation.
2. Steeply dipping N-S foliation.
3. Steeply dipping E-W foliation.
4. Steeply dipping N130° foliation.
5. Steeply dipping N65° foliation.

The shallow dipping foliation was observed towards the north of Madkhol village in location DMY-7 (Fig 4). The rock is a quartz rich garnet muscovite schist which contains recumbent folds on quartzo-feldspathic layers (Fig5). The garnets in this outcrop are sub-mm in size. No linear structural elements were observed within this outcrop.

A penetrative N-S foliation is observed in garnet mica schist at location DMY 5 in the northern part of the study area. The trend of the penetrative foliation varies from N360°-N20° and dips vary from 60° to 70° towards the East. Linear structural elements trending in N-S and dipping in 70° towards east and plunging moderate-steep towards

north & south are recorded within this outcrop, with the Y axes of the elliptical cross sections oriented sub-parallel to the penetrative N-S foliation. The linear structural elements are steeply plunging towards south (Fig 16c). The linear structural elements are usually more resistant than the host schists so they stand out of the rocks due to differential weathering. However, the linear structural elements are never observed to be tapering along their length and the bottom end of these elements is never observed. The steeply-dipping N-S deformation has a sinistral shear sense (Fig 6). The N-S fabric is observed to be transposed into the E-W fabric in the northeastern part of the study area with a sinistral shear sense (Fig 7).

The most dominant foliation in the schists of the area, the E-W foliation, is observed from Gothos to Kunkeri villages covering the central portions of the study area. The strike of the foliation varies from  $90^{\circ}$  to  $120^{\circ}$  and dips steeply to moderately towards the north. Long cylindrical to elliptical linear structural elements have been observed in these outcrops of garnet mica schist. Sheath folds are trending in E-W and plunging moderately towards east. E-W is curving into  $N130^{\circ}$  at Kunkeri and Nivaje villages of the study area. The aspect ratio of these linear structural elements varies from 1.2 to 13.5 (Fig 19). The linear structural elements show concentric zoning with dark and light alternating layers, but the cores of these lineations are usually bright red, indicating the presence of profuse garnets.

Outcrop NC 57 has a penetrative foliation of E-W defined by the alignment of minerals and elliptical lineations present in outcrop. The outcrop has been affected by  $N130^{\circ}$  shears and the low strain domain in the outcrop has preserved a fold defined by these elliptical lineations. The fold is trending in NW-SE direction and plunging moderately towards NW. The plunges of the elliptical lineations exhibit gentle-moderate plunges at the southern limb, steep plunges at the northern limb and steep to gentle plunges at the

hinge of the fold with the steepest plunges closest to the core of the fold. The stereographic projection of the plunges of the coarse lineations defining the intrafolial fold define a great circle girdle trending in NW-SE and fold is moderately plunging towards NW (Fig 16a). the coarse lineations in the penetrative foliation trend in E-W direction and plunge moderately – steeply towards East (Fig 16b).

The E-W foliation has been traversed by N130° shears towards the NE of the study area and E-W is warping into N130°. E-W foliation has also been cross cut by quartz veins trending in N130° (Fig 10).

N130° foliation is present towards the northern part of the study area. This foliation is observed in the dark colored garnet mica schist in the area. The trend varies from 130° to 135° dip varies from 75°-85°. Linear structural elements with Y axes trending N130° plunge steeply towards NW within this fabric.

N65° foliation has been observed in an outcrop at Ambegaon village. The outcrop is of garnet mica schist trend varying from N65°-N70° dipping 78° towards south. Linear structural elements in this foliation trend N65 dipping steeply towards south and steeply plunge towards WSW. Sheath folds in this domain define a larger fold trending in N65°. In the outcrop N130° is intrafolial to N65° foliation (Fig 15: a & b).



**Fig 5:** Section view looking west, of recumbent folds with axial planes describing the shallow dipping foliation in the area



**Fig 6:** Plan view photograph of a calc-silicate layer in a biotite schist showing sinistral shear sense on the N-S foliation..



**Fig 7:** Plan view photograph of a calc-silicate layer in a biotite schist showing sinistral shear sense developed due to the penetrative E-W foliation in the outcrop.



**Fig 8:** Plan view field photograph of a freshly exposed cross section of the linear structural elements in the area. Note the concentric mineralogical layering. Marker measures 14cm and head points north.



**Fig 9:** Plan view photograph with N130° foliation intrafolial to N65° foliation.



**Fig 10:** N130° trending vein cross cutting E-W trending linear structural elements. Note the sinistral shear sense. Plan view.



**Fig 11:** E-W trending reclined fold on a discontinuous calc-silicate layer that shows the elliptical linear structural elements developed in the northern limb. The fold is intrafolial to the penetrative E-W foliation in the outcrop.



**Fig 12:** N130° trending vein cross cutting E-W trending sheath fold and has a sinistral shear sense. Pen head pointing north.



**Fig 13:** Inclined view of linear structural elements showing continuity of a layer that was present before the formation of rods perpendicular to y axis that appears like sheath folds along Y-Z plane.



**Fig 14:** Image of a folded layer with a linear structural element of a similar layer trending parallel to the fold axis of the fold.

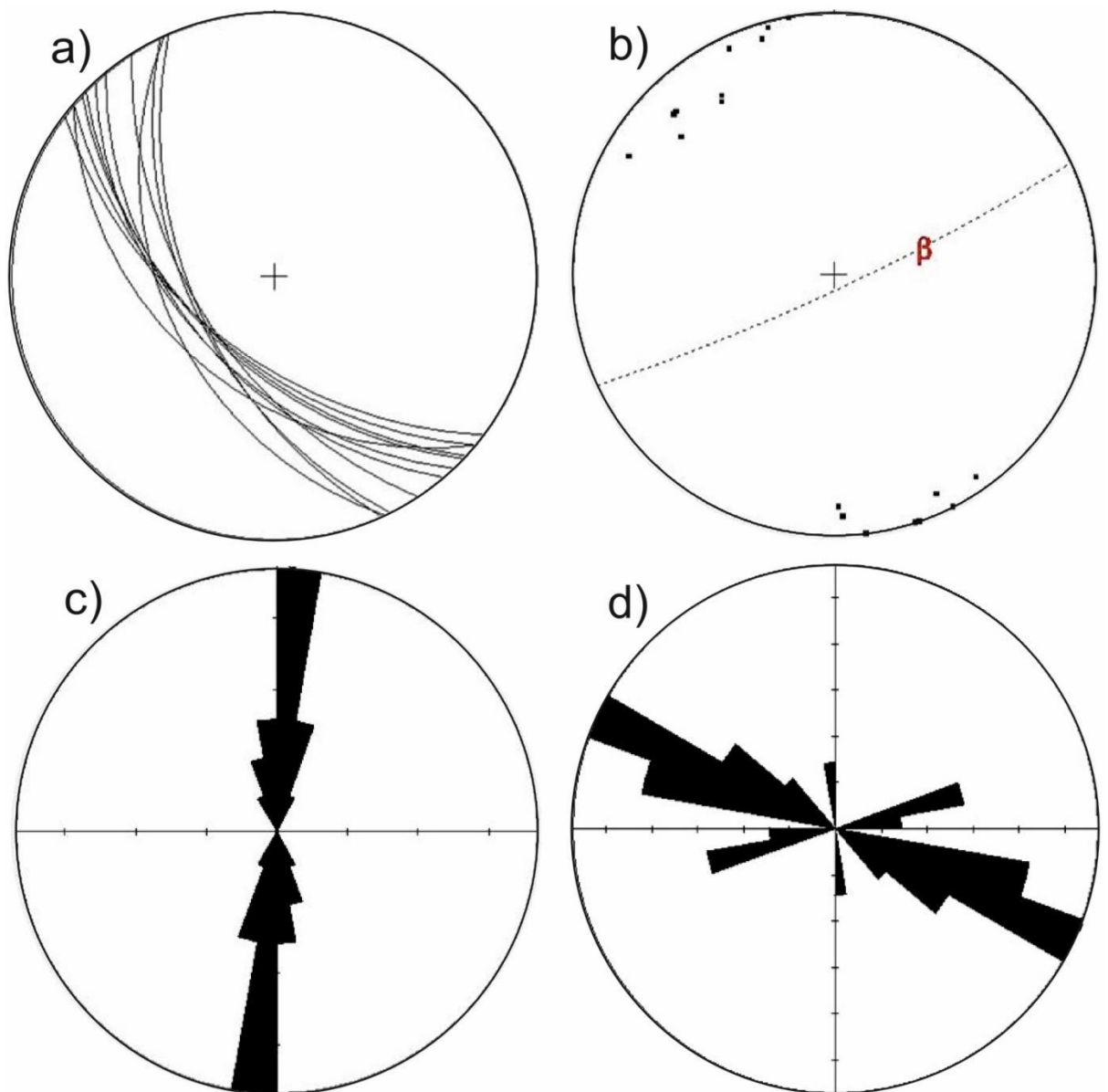


**Fig: 15 a)** Data collected of linear structures trending in N130° dipping moderately towards SW from a low strain domain in outcrop DMY 2. **b)** Poles to planes of data collected on linear structures from high strain domain in outcrop DYM 2 defining a fold trending in N65°. **c)** Rose diagram showing attitude of linear structures trending in N-S direction. **d)** Rose diagram of all the foliations from the study area showing major set trending in N110°-N120° and a subset trending in N65°.

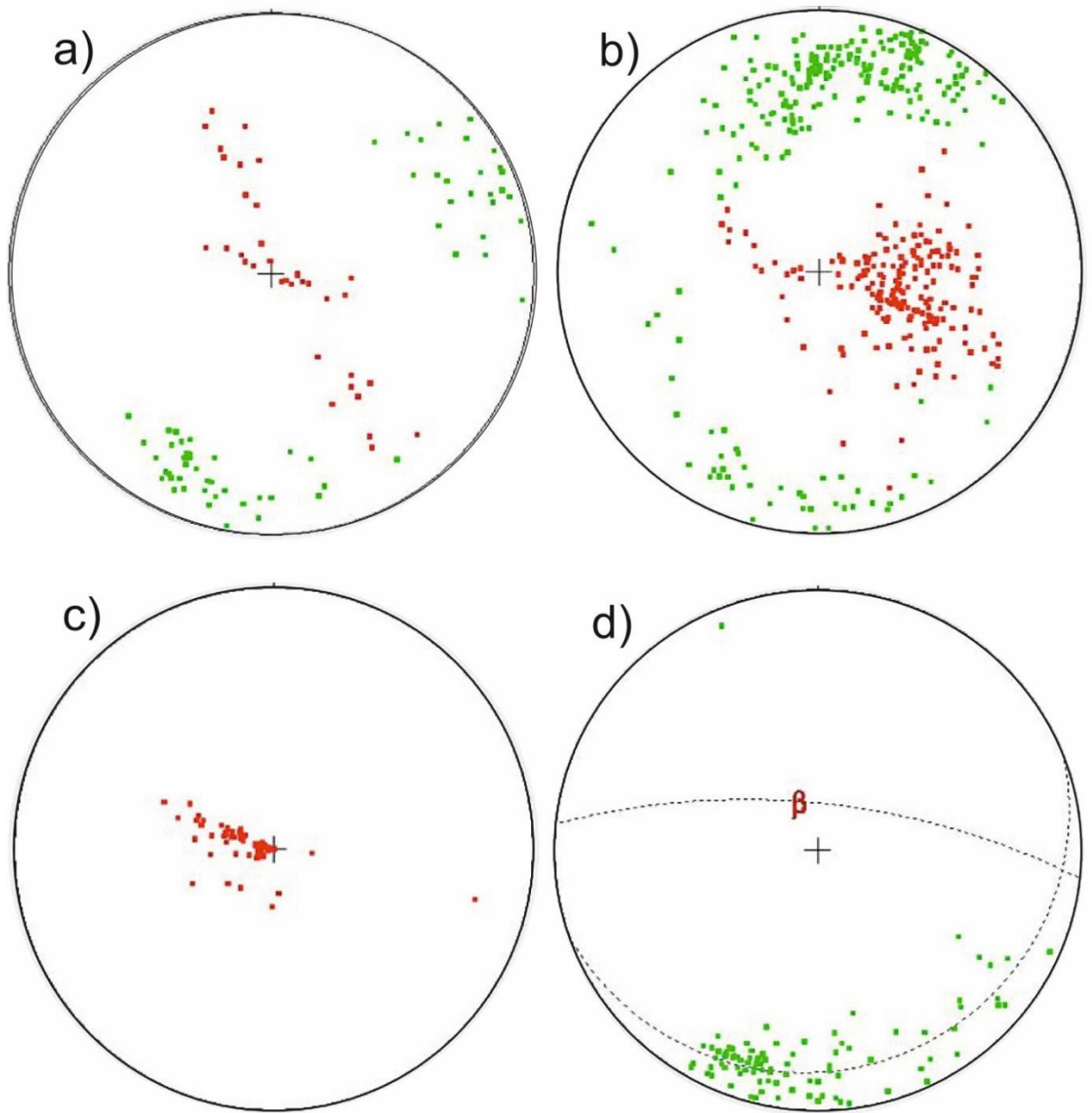


**Fig 16:** Plunges plotted in red and poles to plain plotted in green **a)** data of doubly plunging fold defined by linear structures from low strain domain from outcrop NC 57. **b)** Data on linear structures from high strain domain from outcrop NC 57 plunging moderately-steeply towards east. **c)** Data of linear structures in E-W foliation plunging steeply towards west. **d)** Data of poles to plains of linear structures in E-W foliation.

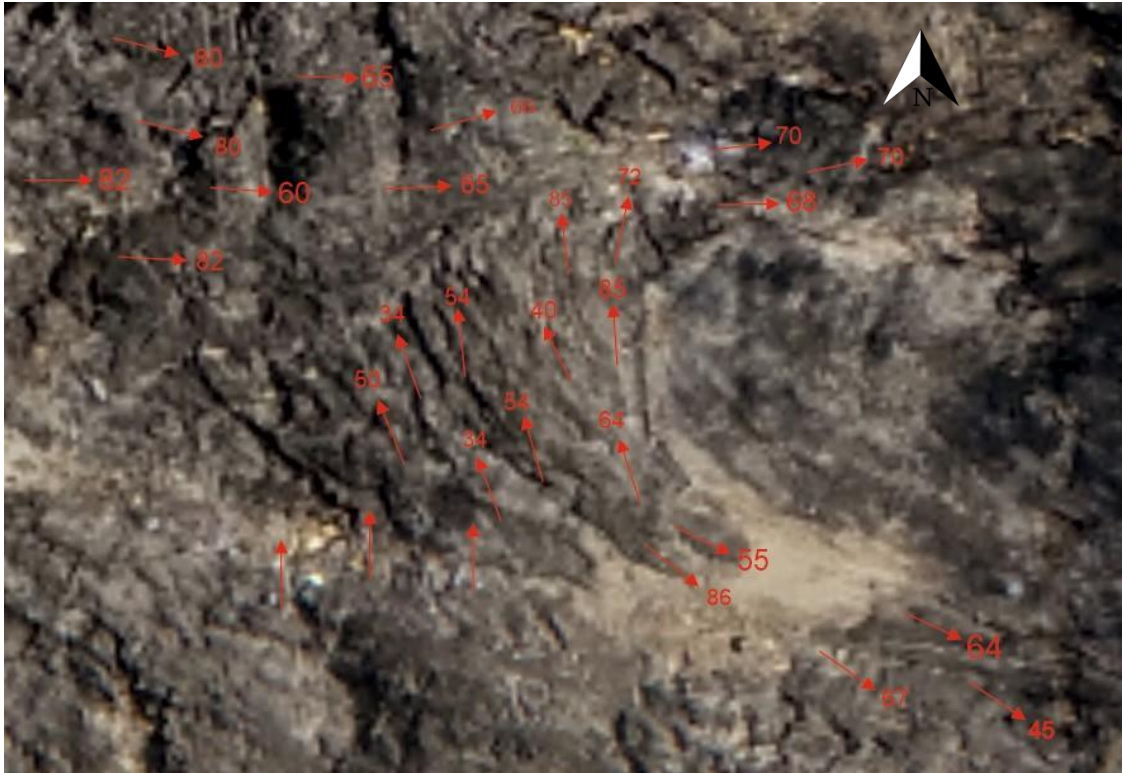


**Fig 17:** Data on coarse lineations showing variation in plunges at the hinge of the fold from core to the periphery defining an intrafolial fold in the E-W foliation in outcrop NC57 plotted on an aerial photograph. The sheath folds are plunging steeply at the core and gently towards the periphery.



**Fig 18:** strike and dip of the coarse lineations defining an intrafolial fold in the E-W foliation in outcrop NC57 marked on an aerial photograph.

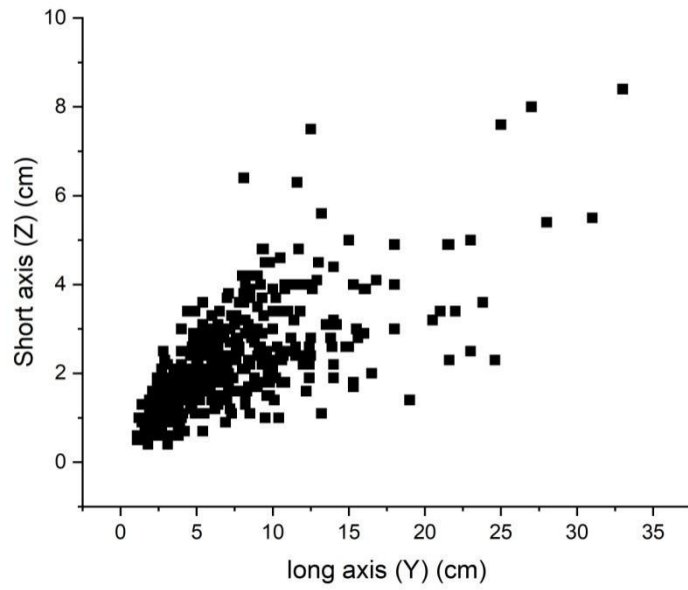


**Fig 19:** Elliptical ratio-Ryz of coarse lineations from the study area. Most coarse lineations have Ryz values ranging from 1-3. The lowest Ryz value is 1.2 and the highest Ryz value is 13.5

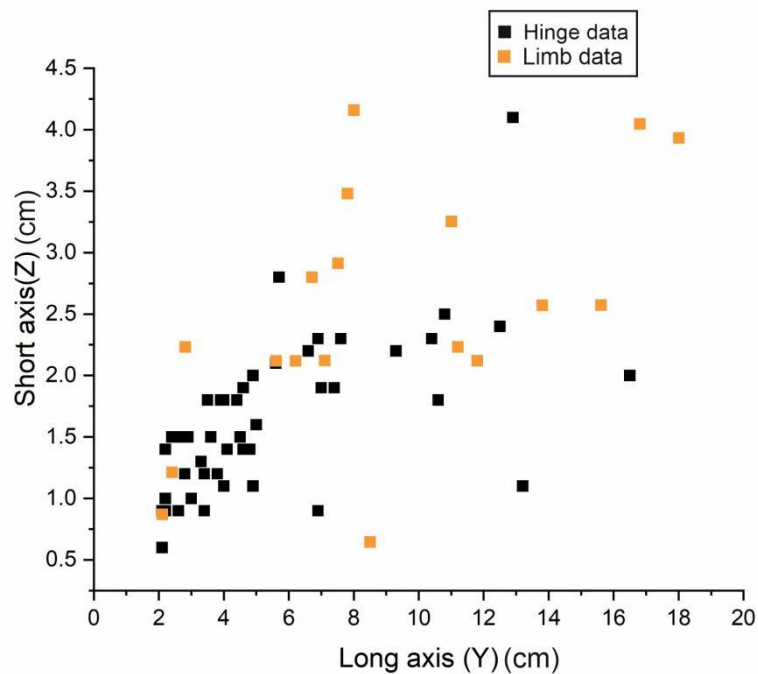


**Fig 20:** Ryz ratios of sheath folds near hinge of the fold data plotted in black and Ryz ratios of sheath folds at the limbs of the fold plotted in yellow. The scatter shows that highest Ryz ratios are towards the hinge to the fold and the sheath folds in the limbs have a lower Ryz ratio.

## **CHAPTER IV**

### **PETROGRAPHIC ANALYSIS**

## **PETROGRAPHY AND MINERAL CHEMISTRY**

The study area is mainly covered with lithologies of Granites overlain by Garnet Mica schist. Garnet mica schist is dark gray in color and has medium sized grains. It consists of Garnet porphyroblast of varying sizes and biotite grains exhibit lepidoblastic texture. The garnet mica schist has mineral assemblage of Garnet + Chlorite + Biotite + Quartz + Feldspar + Ilmenite + Apatite. The Biotite grains exhibit two foliations, the older foliation has been folded and the later foliation is axial planar to these folds. The Granites in the study area are pink and grey in color, form mountain ranges and consist of quartz, feldspars, biotite, hornblende and epidote minerals. These granites are deformed and show alignment of minerals.

## **COARSE LINEATION PETROGRAPHY**

The image (Fig 21) is a section cut perpendicular to the X axis of the coarse lineation. The concentric layers observed in the figure are formed during the formation of the structure and has been divided into three layers based on the change in mineralogy of the layers. The different layers have been marked on the image (Fig 21).

**LAYER 1:** The outermost layer is a hornblende dominant zone and has a mineral assemblage of Quartz + Hornblende + Feldspar + Calcite.

Quartz exhibits undulose extinction. Quartz grains have formed sub grains and subgrain rotation has also occurred. Grain boundary sliding followed by formation of triple junction between adjacent grains is also observed. Material from high strain areas such as grain edges have recrystallized in adjacent low strain areas of the grains resulting in thickening of grain boundaries. Plagioclase is more abundant in this layer exhibiting multiple lamellar twinning and oriented in random direction showing decussate texture. Feldspars have low relief and pitted appearance with straight grain boundaries, sub grains have formed with no proper grain boundary and change in extinction angle

compared to the main grain. Feldspars in this layer vary in composition from Oligoclase to Andesine (Fig 22). Hornblende grains occur as skeletal grains and have subhedral surfaces. Has moderate to high relief, pleochroic from green to brown and has 2 sets of cleavage. Exhibits 2nd order birefringence colors and have symmetrical extinction. Hornblende grains are randomly oriented (Fig 21a). Calcite grains have a low to high relief and shows twinkling effect. The crystals are anhedral and have a rhombohedral cleavage. It is anisotropic and has higher order colors and exhibits symmetrical extinction. These calcite grains are present in a linear manner (Fig 21e) and separates the hornblende dominant layer from the diopside dominant layer.

**LAYER 2:** This layer is present after the hornblende dominant layer and is a few centimeters in thickness. This layer has a mineral assemblage of Hornblende + Pyroxene + Calcite + Feldspar. Pyroxene is pale green in color and has 1 set cleavage with subhedral grain shapes with sinusoidal grain boundaries. Shows higher order birefringence colors with inclined extinction under crossed polarized light. It exhibits a corona texture between Hornblende and pyroxene (Fig 21b). Pyroxene is present at the center and is surrounded by hornblende forming a monomineralic Corona. The pyroxene grains present in this layer have a composition of Mg% 54-58 (Fig 23). Hornblende grains in this layer are smaller compared to Layer 1. Feldspars in this layer are clear compared to the enigmatic grains in the matrix. Feldspars also exhibit zoning and the layer is devoid of quartz.

**LAYER 3:** This layer makes up the core of the coarse lineations, the radius varies in different coarse lineations. The mineral assemblage of this layer is Pyroxene + Feldspar + Calcite + Garnet + Epidote + Apatite + Sphene + Magnetite.

The core consists of skeletal garnets having high relief with inclusions and is isotropic under crossed polars (Fig 21f). Pyroxene reaction rims are observed around garnets

grains in the core. Garnets in the core are Ca and Fe Rich (Fig 24) and are set in a matrix of fibrous Calcite grains. Medium to fine grained euhedral crystals of epidote are present in the layer (Fig 21c). Titanite crystallizes in monoclinic crystal system, is light brown to brown colored mineral forming euhedral crystals and has one set of cleavage. The feldspars in this layer have undergone saussuritization and have formed clay minerals. Zoning is observed in Feldspar grains, Most of the Feldspars in this layer are Andesine. Plagioclase grains get rich in Ca towards the center of the coarse lineations (Fig 22). Composition of pyroxenes in the core varies from Fe% 38-65.

#### **HOST ROCK MINERALOGY.**

Coarse lineations are set in a matrix of garnet biotite schist having a mineral assemblage of biotite + garnet + quartz + feldspar + epidote + apatite + ilmenite. The biotite grains are medium grained and define the foliation of the rock (Fig 21g). Garnets are present as skeletal grains having inclusion of quartz & biotite (Fig 21d).

Biotite, a phyllosilicate mineral with a flexible layering of silica tetrahedra and aluminum-oxygen octahedra, is the most abundant mineral in the matrix. It is a flaky brown mineral having one set of cleavage, brown in color and is pleochroic from light brown to brown in plane polarized light. Under crossed polars it shows straight extinction and 2<sup>nd</sup> order interference colors. The biotite grains are euhedral to subhedral in shape with straight grain boundaries. These Biotites with conspicuous lepidoblastic texture are used to identify the direction and intensity of deformation. Biotites have a uniform composition throughout the matrix (Fig 25). Quartz is colorless in plane polarized light with low relief and shows grey to yellow 1<sup>st</sup> order interference colors and have undulose extinction in BxP. The grains are subhedral to anhedral and most grains have a sinusoidal grain boundary with a few grains having straight boundary. Due to increase in strain, large quartz grains have formed subgrains indicated by the

change in extinction angle of the adjacent grains having slightly developed grain boundary between the subgrains. Chlorite grains are observed scattered throughout the matrix. It is green in color and exhibits pleochroism from pale green to green and has one set of cleavage. It shows 1<sup>st</sup> order birefringence colors and has straight to low angle extinction. The grains are aligned in the direction of the penetrative foliation of the rock. Plagioclase grains are sparsely present within the matrix. It is colorless and has low to moderate relief. It exhibits 1<sup>st</sup> order gray interference colors. Multiple lamellar twinning is also observed in these grains. Plagioclase grains in this layer are Na rich and plots in the Oligoclase zone of the Feldspar ternary plot (Fig 22). K-feldspar shows a pitted appearance having low relief in plane polarized light. Under crossed polars feldspar grains show 1<sup>st</sup> order gray birefringence colors and have straight extinction. These grains have a sinusoidal grain boundary and have undergone the process of saussuritization and have formed clay minerals in some spots. Ilmenite is a black metallic platy mineral which crystallizes in a trigonal crystal system. It is brown in color with high relief. Under crossed polars it is anisotropic and shows first order gray birefringence colors. Apatite occurs as small euhedral to subhedral elongate prismatic crystals. It is colorless with 1 set cleavage and moderate relief in plane polarized light. Under crossed polars it exhibits 1st order interference colors and has parallel extinction. Garnet grains are in skeletal form. Garnets have high relief and colorless in plane polarized light with inclusions of Quartz, Biotite and Feldspars. It is isotropic under crossed polars. Garnets in the matrix have a composition of Fe>>> Mg, Mn, and Ca (Fig 24).

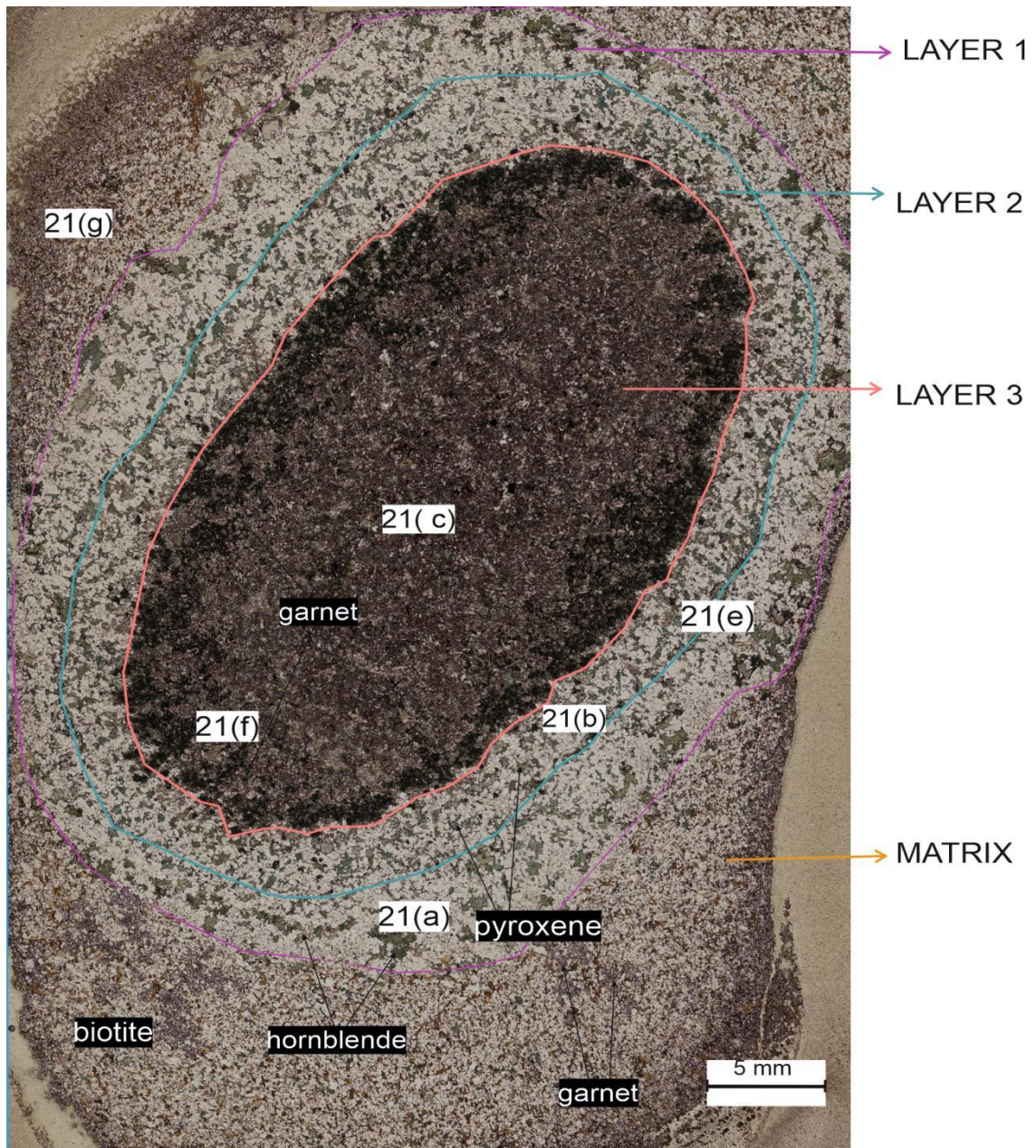


**Fig 21:** PPL photomicrograph of cross section of linear structural element showing concentric layering. Each layer is labelled. Locations of images of the detailed textures (Fig 21 b-g) are keyed to the figure

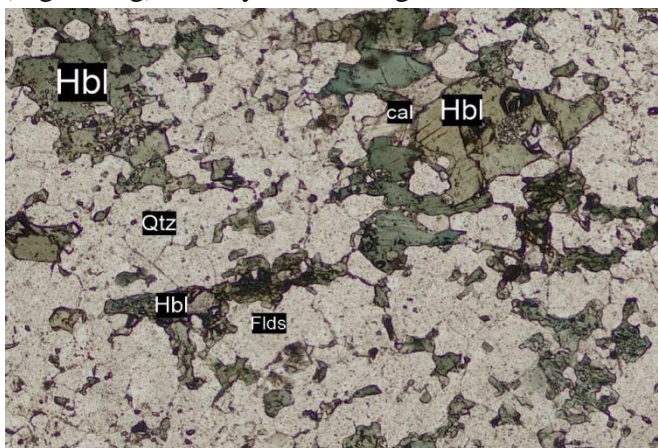


**Fig 21(a):** Plane polarized photomicrograph showing large hornblende grains from layer 1 having no preferred orientation.

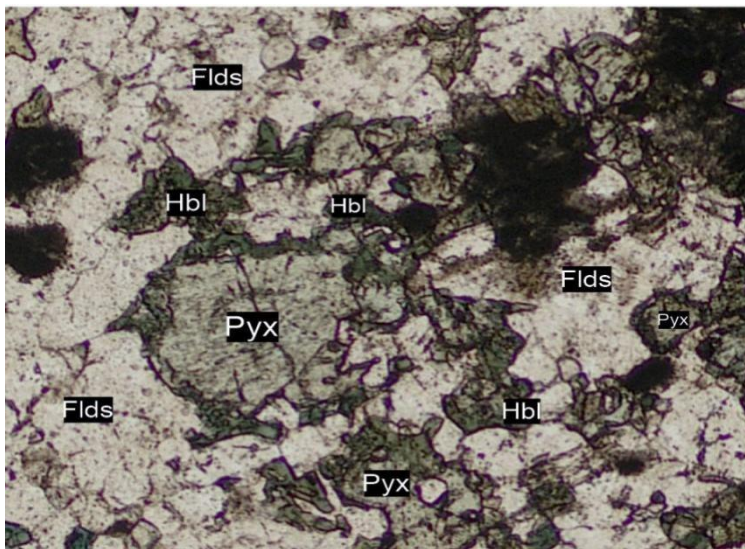


**Fig 21(b):** Plane polarized photomicrograph showing corona texture observed between hornblende and pyroxene in layer 2.

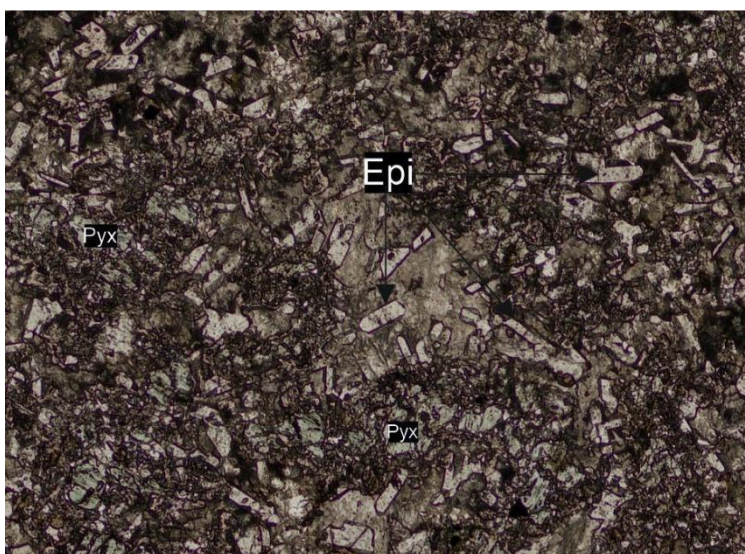


**Fig 21(c):** Plane polarized photomicrograph showing Euhedral crystals of epidote from the center of the coarse lineation.

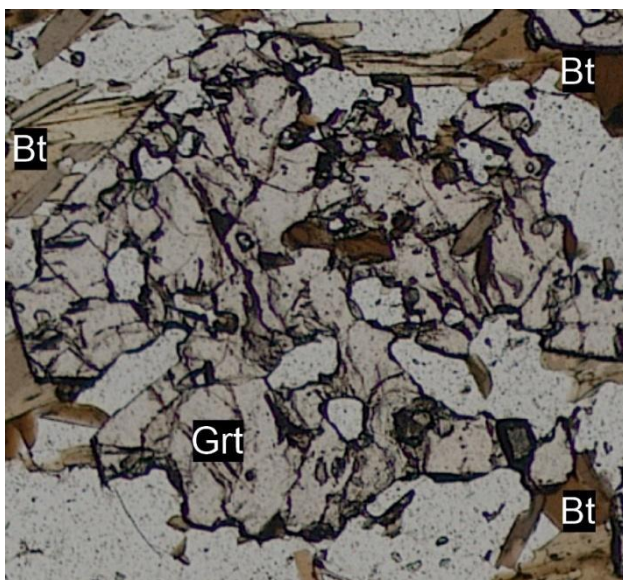


**Fig 21(d):** Plane polarized photomicrograph focused on skeletal garnet from the matrix.

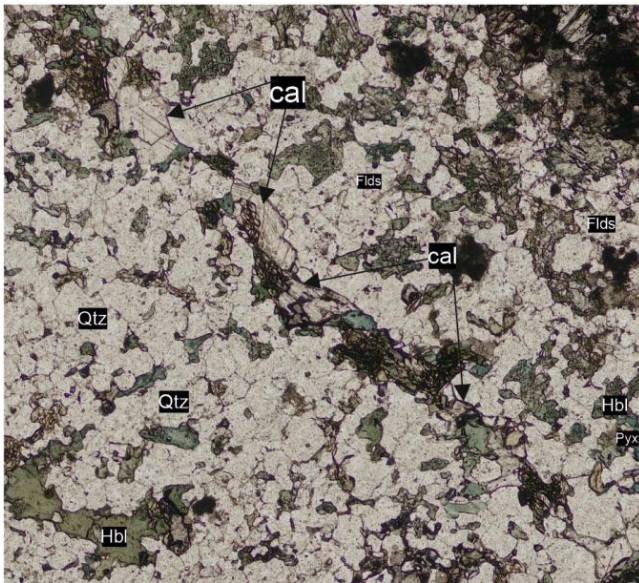


**Fig 21(e):** Plane polarized photomicrograph showing calcite grains separating pyroxene dominant zone from hornblende dominant zone.

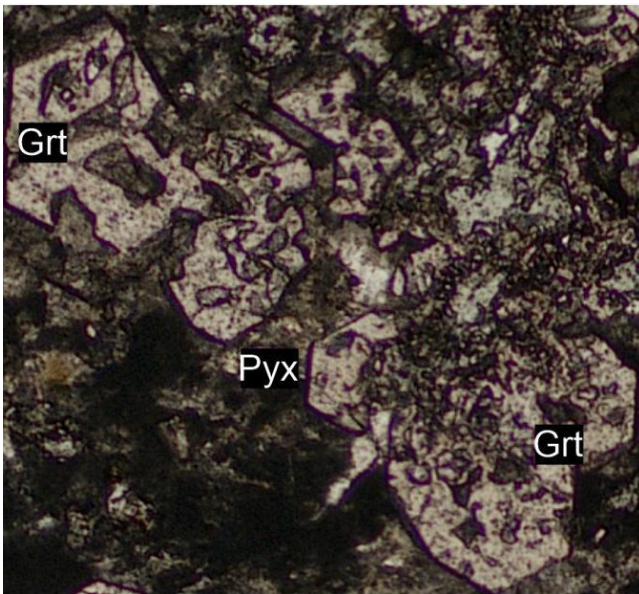


**Fig 21(f):** Plane polarized photomicrograph showing garnet grains from layer 3 of the coarse lineation.

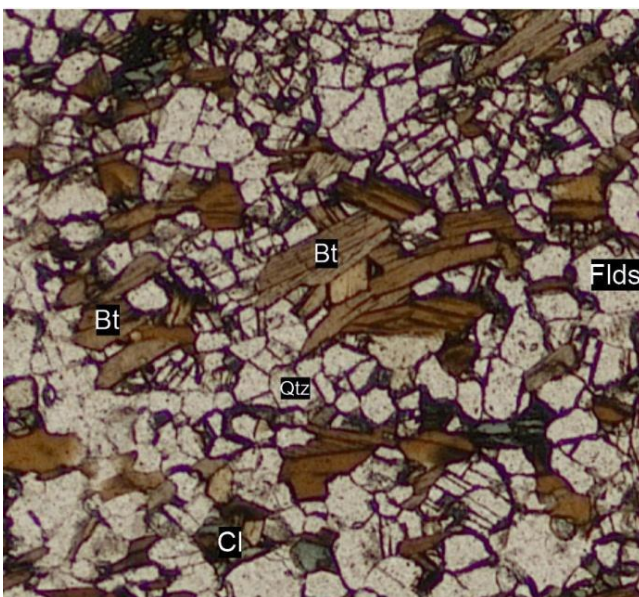


**Fig 21 (g):** Plane polarized photomicrograph showing warping foliation defined by biotites.

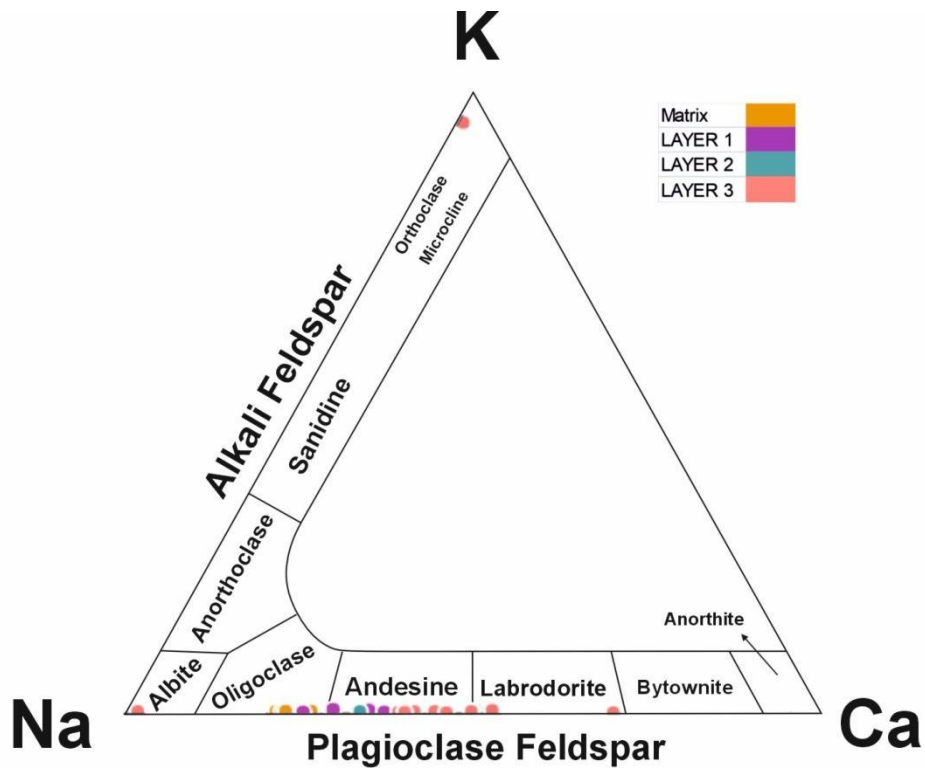


Fig 22: Feldspar anorthite, orthoclase, and albite ternary diagram with compositional subdivisions. compositional variation from the matrix of the coarse lineations and different layers. The matrix consists of Oligoclase feldspars and Ca% increases from layer 1 to layer 3.

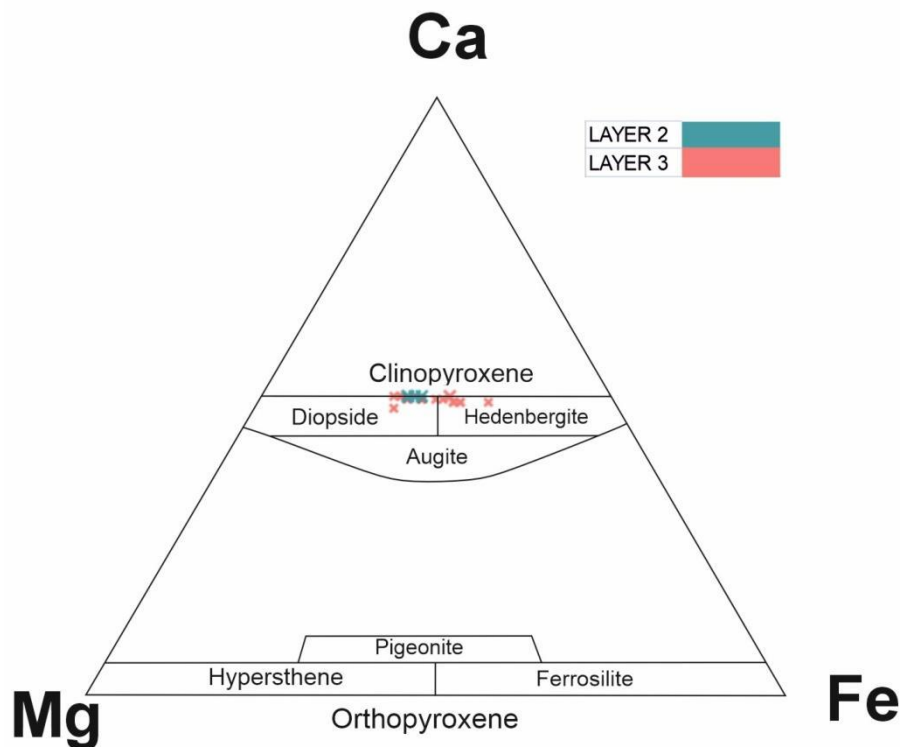
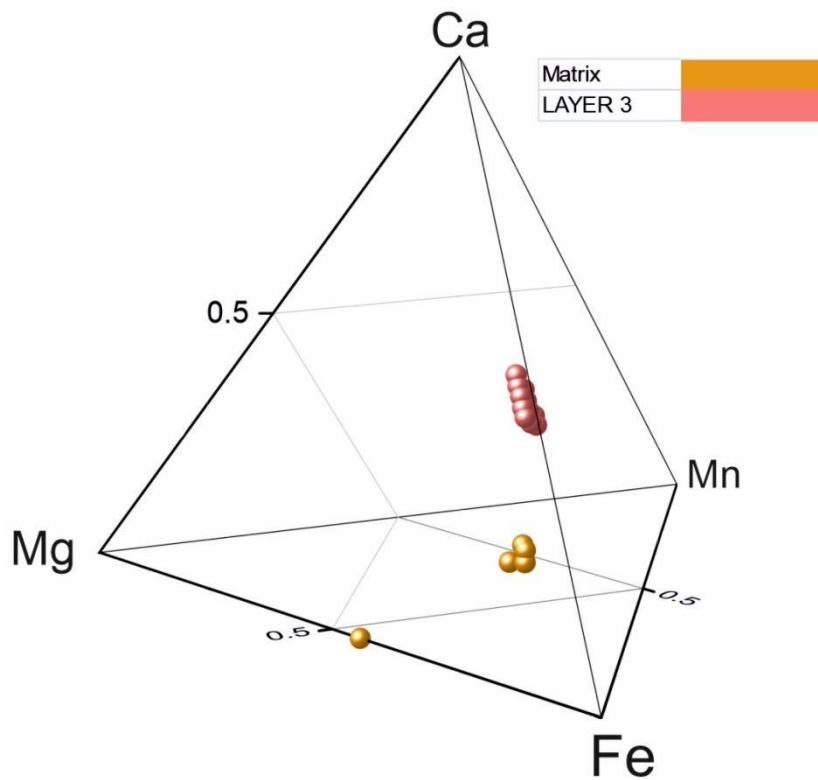
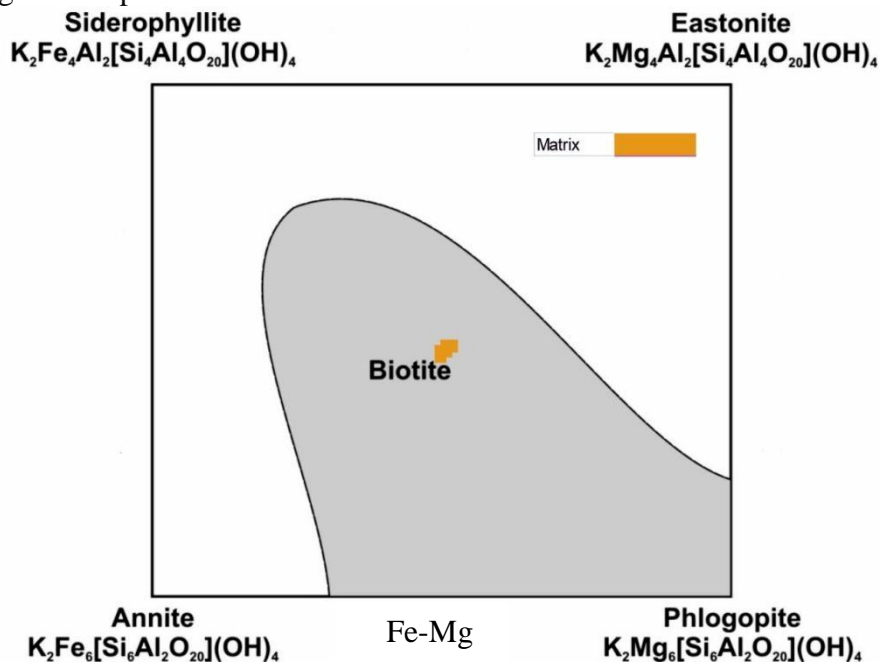


Fig 23: Plot of  $Ca \pm Mg \pm Fe$  pyroxene data on ternary classification diagrams with distinguished pyroxene names. Classification by Morimoto et al. (1988). with layer 2 having Mg% 54-58 and layer 3 Fe% varies from 38-65.



**Fig 24:** Classification diagram for matrix and Layer 3 garnets. Matrix garnets have composition of Mg, Mn, Fe & Ca. layer 3 Garnets Fe-Ca composition with one point having Mg-Fe composition.



**Fig 25:** Compositional plot of biotite in the phlogopite–annite–siderophyllite–eastonite system (Deer et al.1992). The matrix biotites have uniform composition of Fe% 49-51.

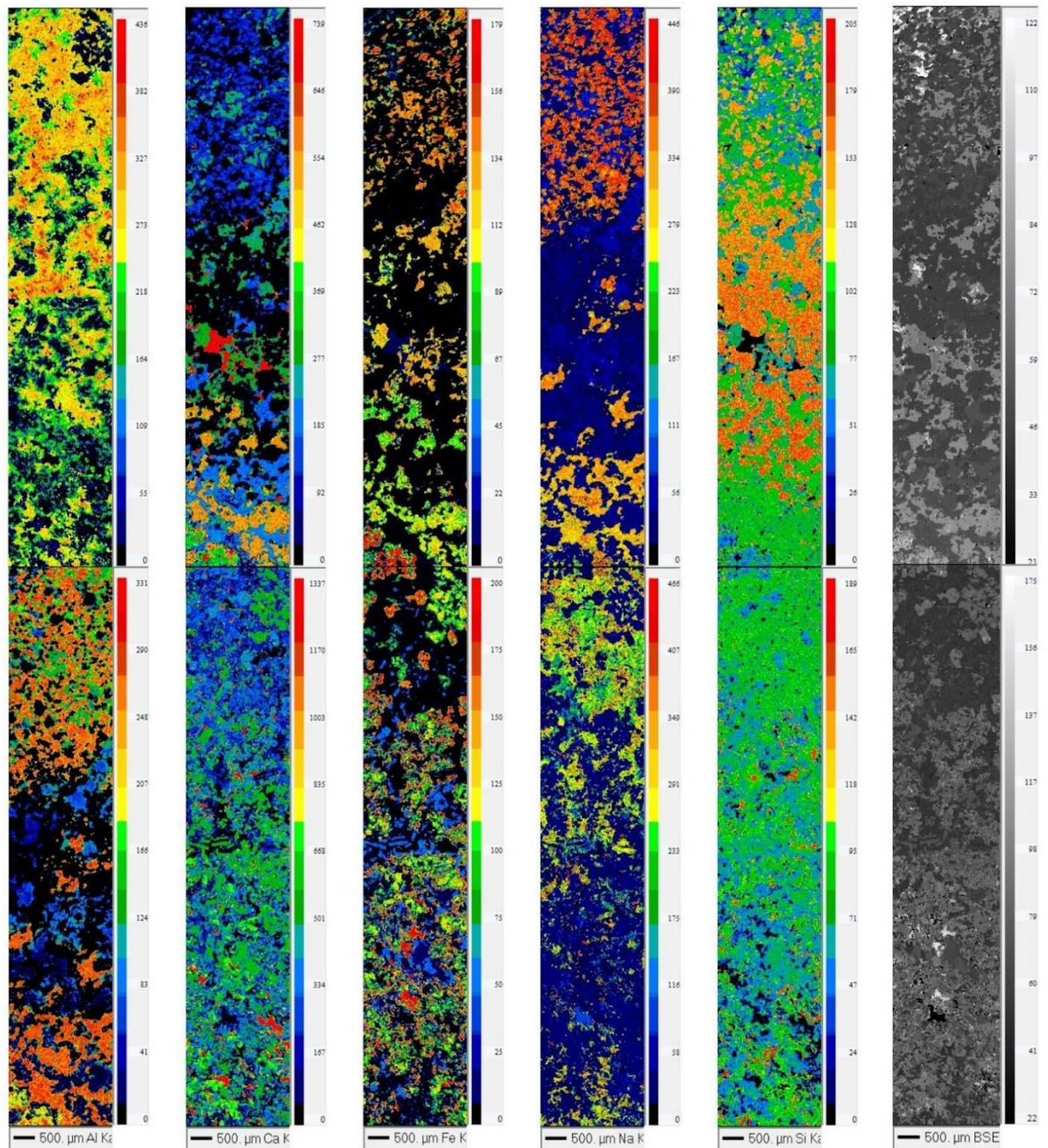


**Fig 26:** Al, Ca, Fe, Na and Si X-ray element maps of the sheath fold from the garnet biotite schist. The matrix is composed of high Na with moderate Si content and Al & Fe content more than moderate and is depleted in Ca content. Layer 1 has high Si content with moderate Al & Fe content. It has low Ca content and is depleted in Na. layer 2 has very high Fe content in some spots and moderate Fe content in the other spots. It has high Al content and moderate Ca, Na and Si content. The outer part of layer 3 has moderate Ca and Si content, and is depleted in Fe excluding a few spots with high Fe content. It is depleted in Na and Al. The inner part of layer 3 has similar content for Ca, Fe, Na and Si but is enriched in Al.

**Table 1:** Electron Probe micro analytical data and structural formula for pyroxene on the basis of 6 oxygens.

SiO <sub>2</sub>	52.89	52.42	52.9	52.66	51.4	52.69	51.52	53.07	51.78
Al <sub>2</sub> O <sub>3</sub>	0.55	0.61	0.54	0.63	0.98	0.88	0.95	0.87	0.2
TiO <sub>2</sub>	0.01	0.05	0.02	0	0.04	0	0	0.08	0.05
FeO	13.64	14.01	12.99	12.91	17.33	12.91	16.4	12.29	17.15
MnO	0.61	0.5	0.62	0.54	0.66	0.32	0.38	0.22	0.82
MgO	9.61	9.35	10.07	9.95	7.18	9.96	7.72	10.46	7.84
CaO	23.92	23.63	23.76	23.96	22.74	23.83	23.36	24.05	23.51
total	101.5	100.9	101.18	101.0	100.69	100.91	100.7	101.3	101.5
Si	2	2	2	2	2	2	2	2	2
Al	0	0	0	0	0	0	0	0	0
Ti	0	0	0	0	0	0	0	0	0
Fe	0.4	0.4	0.4	0.4	0.6	0.4	0.5	0.4	0.6
Mn	0	0	0	0	0	0	0	0	0
Mg	0.5	0.5	0.6	0.6	0.4	0.6	0.4	0.6	0.4
Ca	1	1	1	1	0.9	1	1	1	1
Xfe	0.44	0.46	0.42	0.42	0.58	0.42	0.54	0.4	0.55

**Table 2:** Electron Probe micro analytical data and structural formulae for Garnets. On the basis of 12 oxygens.

SiO <sub>2</sub>	38.2	37.9	38.4	37.5	38.2	38	35.8	38.3
Al <sub>2</sub> O <sub>3</sub>	21	21.1	21.2	20.8	21	21	15.4	21.1
TiO <sub>2</sub>	0.2	0.1	0	0	0.1	0	3	0
FeO	21.7	21.7	22.1	20.8	28.7	29.4	21.7	29.5
MnO	2.9	2.9	2.3	2.2	3.1	3.2	0.2	3.3
MgO	1.1	1	1.2	1	2.9	3	9.1	2.7
CaO	16.3	15.8	16	17.4	6.9	6.5	0.2	6.7
Total	101.2	100.6	101.1	99.7	100.9	101.1	85.6	101.6
Si	3	3	3	3	3	3	3	3
Al	1.9	2	2	1.9	2	2	1.5	2
Ti	0	0	0	0	0	0	0.2	0
Fe	1.4	1.4	1.4	1.4	1.9	1.9	1.5	1.9
Mn	0.2	0.2	0.2	0.1	0.2	0.2	0	0.2
Mg	0.1	0.1	0.1	0.1	0.3	0.4	1.2	0.3
Ca	1.4	1.3	1.3	1.5	0.6	0.5	0	0.6
Xfe	0.46	0.47	0.47	0.44	0.62	0.63	0.56	0.64
XMg	0.04	0.04	0.04	0.04	0.11	0.12	0.42	0.1
Xca	0.44	0.43	0.44	0.47	0.19	0.18	0.01	0.19
XMn	0.06	0.06	0.05	0.05	0.07	0.07	0.01	0.07

**Table 3:** Electron Probe micro analytical data and structural formulae for feldspars on the basis of 8 oxygens.

SiO <sub>2</sub>	61.6	63.5	61.2	61	58.8	58.5	67.7	57.9
Al <sub>2</sub> O <sub>3</sub>	24.1	24	24.9	25	26.8	26.67	19.8	27.6
TiO <sub>2</sub>	0	0	0	0	0	0.04	0	0.1
FeO	0.1	0	0	0	0.1	0.01	0.2	0.1
MnO	0	0	0	0	0	0	0	0
MgO	0	0	0	0	0	0	0	0
CaO	5.6	5	6.3	6.4	8.4	8.63	0.6	9.4
Na <sub>2</sub> O	9	9.6	8.6	8.6	7.3	7.2	11.9	6.8
Total	100.3	102.2	101.1	101.2	101.5	101.1	100.3	101.8
Si	2.7	2.8	2.7	2.7	2.6	2.6	3	2.6
Al	1.3	1.2	1.3	1.3	1.4	1.4	1	1.4
Ti	0	0	0	0	0	0	0	0
Fe	0	0	0	0	0	0	0	0
Mn	0	0	0	0	0	0	0	0
Mg	0	0	0	0	0	0	0	0
Ca	0.3	0.2	0.3	0.3	0.4	0.4	0	0.4
Na	0.8	0.8	0.7	0.7	0.6	0.6	1	0.6
Xna	0.74	0.78	0.71	0.71	0.61	0.6	0.98	0.57

**Table 4:** Electron Probe micro analytical data and structural formulae for biotites. On the basis of 11 oxygens.

SiO <sub>2</sub>	36.83	37.69	36.93	38.06	37.21	37.26	37.02
Al <sub>2</sub> O <sub>3</sub>	15.79	16.17	15.68	15.91	15.48	15.93	15.6
TiO <sub>2</sub>	2.77	2.8	2.73	2.34	2.82	2.92	2.78
FeO	19.83	19.34	20.18	19.71	20.16	19.76	19.89
MnO	0.05	0.14	0.04	0.09	0.13	0.09	0.07
MgO	10.84	10.65	10.7	11.12	10.58	10.62	10.63
CaO	0.1	0.11	0	0.13	0.07	0.06	0
Na <sub>2</sub> O	0.3	0.35	0.32	0.32	0.31	0.27	0.31
K <sub>2</sub> O	8.54	8.28	8.77	8.24	8.47	8.53	8.8
Total	95.43	95.95	95.71	96.24	95.55	95.73	95.36
Si	2.8	2.8	2.8	2.9	2.8	2.8	2.8
Al	1.42	1.4	1.4	1.4	1.4	1.4	1.4
Ti	0.16	0.2	0.2	0.1	0.2	0.2	0.2
Fe	1.26	1.2	1.3	1.2	1.3	1.2	1.3
Mn	0	0	0	0	0	0	0
Mg	1.23	1.2	1.2	1.2	1.2	1.2	1.2
Ca	0.01	0	0	0	0	0	0
Na	0.04	0.1	0	0	0	0	0
K	0.83	0.8	0.9	0.8	0.8	0.8	0.9
Xfe	0.51	0.5	0.51	0.5	0.52	0.51	0.51
Al <sup>IV</sup>	0.51	0.59	0.51	0.52	0.52	0.55	0.53

## **CHAPTER V**

### **GEOHERMOBAROMETRY**

## **GEOOTHERMOBAROMETRY.**

Temperatures were estimated from Garnet-Biotite pairs in the matrix using the thermometric formulations proposed by Bhattacharya et al. (1992), Dasgupta et al. (1991), Ferry and Spear (1978), 5) Hodges and Spear (1982), 6) Perchuk et al. (1991) 7) Thomas et al. (1976). For layers 1-3 and matrix wherever possible, garnet-hornblende thermometer formulations by Graham & Powell (1984) and Perchuk (1991) were used as well as Hornblende-Plagioclase pairs using formulation by Holland & Blundy (1994b), Hornblende-Plagioclase-Quartz formulation by Holland & Blundy (1994a) and Garnet - Clino-Pyroxene thermometric formulations proposed by Nakamura (2009). Estimation of pressures were done by using Hornblende-Plagioclase barometer by Bhadra & Bhattacharya (2007) and Molina et al. (2015), Garnet-Hornblende-Plagioclase-Quartz (GHPQ) and Garnet-Clinopyroxene-Plagioclase-Quartz formulation by Eckert, Newton & Klepeš (1991).

Most thermometric formulations for garnet-biotite pairs provided temperature ranging from 595°C -615°C except for Dasgupta et al. (1991) provided a lower temperature of 589°C and Hodges and Spear (1982) and Thomas et al. (1976) provided comparatively higher temperatures of 673°C & 624°C respectively for the matrix. Garnet-Hornblende thermometers provided temperatures ranging from 606°C -612°C for matrix. Hornblende-Plagioclase thermometer calculated temperature was 605°C for matrix 621°C for Layer 1 & layer 2. Hornblende-Plagioclase-Quartz thermometer provided a temperature value of 615°C for matrix, 624°C for layer 1 and 627°C for layer 2. Garnet-Clinopyroxene thermometer provided a temperature of 685°C for layer 3.

Pressures estimated using Hornblende-Plagioclase barometric formulation by Bhadra & Bhattacharya (2007) yielded 7.75kbar for matrix, 8.5kbar for layer 1 and 7.4kbar for layer 2. Molina et al. (2015) provided temperature value of 8.5kbar for matrix, 7.7kbar

for layer 1 and 8.2kbar for layer 2. GHPQ barometer yielded 8.4kbar for matrix.

Granet-Clinopyroxene-Plagioclase-Quartz barometer provided 8.3kbar for layer 3.

**Table 5:** 1)&2)Bhattacharya et al. (1992) using mixing parameters GS-Ganguly and Saxena (1984), HW-Hackler and Wood (1989); 3) Dasgupta et al.(1991); 4)Ferry and Spear (1978); 5) Hodges and Spear (1982); 6) Perchuk et al.(1991) :7) Thomas et al.(1976); 8) Graham & Powell (1984); 9) Perchuk (1991); 10) Holland & Blundy (1994)b; 11) Holland & Blundy (1994)a; 12)Nakamura(2009).

<b>Temperature ( °C ) at 7.5kbar</b>	<b>Pairs used</b>	<b>No</b>	<b>Matrix</b>	<b>Layer 1</b>	<b>Layer 2</b>	<b>Layer 3</b>
	<b>Garnet Biotite</b>	<b>1</b>	<b>614</b>	-	-	-
		<b>2</b>	<b>611</b>	-	-	-
		<b>3</b>	<b>589</b>	-	-	-
		<b>4</b>	<b>602</b>	-	-	-
		<b>5</b>	<b>673</b>	-	-	-
		<b>6</b>	<b>597</b>	-	-	-
		<b>7</b>	<b>624</b>	-	-	-
	<b>Grt-Hbl</b>	<b>8</b>	<b>606</b>	-	-	-
		<b>9</b>	<b>612</b>	-	-	-
	<b>Hbl-Pl</b>	<b>10</b>	<b>605</b>	<b>621</b>	<b>621</b>	-
	<b>Hbl- Pl(Qtz)</b>	<b>11</b>	<b>615</b>	<b>624</b>	<b>627</b>	-
	<b>Grt- Cpx</b>	<b>12</b>	-	-	-	<b>685</b>

**Table 6:** 13) Bhadra & Bhattacharya (2007):14) Molina et al. (2015):15) kohn & spear (1989):16) Eckert, newton & kleppa (1991).

<b>Pressure (kbar) at 600°C</b>				
<b>Pairs used</b>	<b>Hbl-Pl</b>		<b>GHPQ</b>	<b>Grt- Cpx- Pl(Qtz)</b>
<b>No</b>	<b>13</b>	<b>14</b>	<b>15</b>	<b>16</b>
<b>Matrix</b>	<b>7.75</b>	<b>8.5</b>	<b>8.4</b>	<b>-</b>
<b>Layer 1</b>	<b>8.5</b>	<b>7.7</b>	<b>-</b>	<b>-</b>
<b>Layer 2</b>	<b>7.4</b>	<b>8.2</b>	<b>-</b>	<b>-</b>

## **CHAPTER VI**

### **DISCUSSION & CONCLUSION**

## DISCUSSION & CONCLUSION

The coarse linear structures in the Sawantwadi area of Sindhudurg have been reported as sheath folds in all previous studies (Rekha and Bhattacharya, 2014; Azhar 2021; Venugopal, 2023). However, the structural and petrological characteristics reported in the present study indicate that this assumption may not be true.

Both in field and in thin section, the host rock mineralogy is not repeated in the multiply layered coarse lineation. This is uncommon in sheath as sheath folds which form along a slip plane and can be multilayered but the host rock mineralogy will be present within the sheath folds.

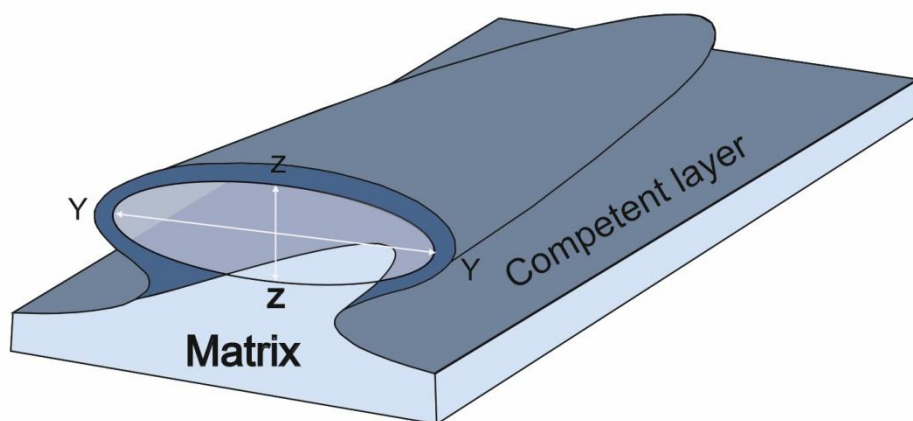


**Fig 27:** Formation of sheath fold around a competent layer modified after Marques et al. (2008)

According to Skjernaa (1989) definition, The hinges of sheath folds are sub-parallel, and parallel to a prominent mineral stretching lineation which is not seen in the sheath folds in the study area. Fig 13 and Fig 14 show how the formation of different layers with the rods make them appear like sheath folds along the Y-X plane but shows clear continuity of earlier layers which would not be the case if they were sheath folds.

The geothermobarometry analysis of the individual layers and the matrix suggest that minerals in the matrix equilibrated at lower temperature of 605°C -615°C and the layer 1 & 2 of the rods equilibrated at temperature ranging from 620°C -630°C and minerals in layer 3 equilibrated at higher temperature of 685°C with pressure ranging from 7.5-8.5kbar across all the layers of the rods and matrix. Change in temperature within different layers of the same rock could be due to hydrothermal fluid injection in the calc-silicate layers which led to rheological contrast in the calc-silicate layer and the matrix of garnet biotite schist. It is therefore inferred that during deformation, the calc-silicate bands acted as competent layers and led to rodding of the layers and the matrix of garnet biotite schist acted as incompetent layer and would flow along the deformation direction while the y axis of the rods would align in the direction of the later deformation events. The garnet biotite schist in the study area is intruded by granite batholiths hence the hydrothermal fluids intruded in the rock could be from these granites making these layers a skarn deposit.

The petrography and mineral chemistry analysis of the rods shows change in mineralogy. Layer 1: Hornblende + plagioclase + quartz. Layer 2: diopside (with hornblende coronas) + quartz+ plagioclase. Layer 3: garnet + diopside + epidote + plagioclase + calcite + titanite. Host rock mineralogy is biotite + quartz + plagioclase ± garnet ± hornblende.

Based on the Classification of rods by (Martins-Ferreira & Rodrigues 2021) rods in the study area found at the limbs of the fold are elliptical as the relations of the strain ellipsoid axes are  $Z < Y < X$ . The rods at the hinge of the fold are tabular rods as the relations of the strain ellipsoid axes are  $Z \ll Y < X$ .

According to Martins-Ferreira & Rodrigues (2021), the much longer x-axis of the strain ellipsoid in rods suggests constrictional deformation. The rods in the study area have axis length  $Z < Y < X$  hence the rods have formed due to constrictional deformation. Rods can assume an elliptical shape in the yz basal plane, where  $y \gg z$  and fall into the flattening or oblate deformation fields, This is observed in Ryz ratios of rods at the hinge of the folds (Fig 20).

The plunges of the Rods in N130 & N65 foliation vary and rods define a fold, hence these foliations are post-rod foliation and has no genetic relationship to rods. The rods in N-S foliation are doubly plunging hence the rods either formed during progressive N-S deformation or before N-S deformation. The rods in penetrative E-W foliation plunge moderately towards East and all rods have same plunge so they either formed during E-W deformation event or aligned in the direction of the deformation.

## **CONCLUSION**

Rods are found throughout the study area. The geometry of the rods differs from the hinges to the limbs of the folds with higher Ryz ratios at the hinge of the folds and lower Ryz ratios towards the limbs. The rods have been divided into 3 layers based on the change in mineralogy. Petrographic analysis indicates that the lineations have concentric layers with varying mineralogy: From core to rim, Layer 1: Hornblende + plagioclase + quartz. Layer 2: diopside (with hornblende coronas) + quartz + plagioclase. Layer 3: garnet + diopside + epidote + calcite + titanite. Host rock mineralogy is biotite + quartz + plagioclase  $\pm$  garnet  $\pm$  hornblende. Combining the different datasets it is concluded that the linear structures are rods that have developed from interbanded calc-silicate layers in the biotite schist, and not sheath folds. The rodding possibly initiated during the N-S foliation formation but also progressed during

the later deformations. This indicates that rheologic differences in protoliths control the formation of linear stretching structures developed within progressively deformed amphibolite facies metamorphic schists.

## REFERENCES

- Alsop, G. I., & Holdsworth, R. E. (2006). Sheath folds as discriminators of bulk strain type. *Journal of Structural Geology*, 28(9), 1588-1606.
- Berthé, D., Choukroune, P., & Jiangwei, Z. (2001). Porphyroclasts and their role in the kinematic analysis of shear zones. *Journal of Structural Geology*, 23(12), 1633-1643.
- Bhadra, S., & Bhattacharya, A. (2007). The barometer tremolite+ tschermakite+ 2 albite= 2 pargasite+ 8 quartz: Constraints from experimental data at unit silica activity, with application to garnet-free natural assemblages. *American Mineralogist*, 92(4), 491-502.
- Bhattacharya, A., Mohanty, L., Maji, A., Sen, S. K., & Raith, M. (1992). Non-ideal mixing in the phlogopite-annite binary: constraints from experimental data on Mg-Fe partitioning and a reformulation of the biotite-garnet geothermometer. *Contributions to mineralogy and petrology*, 111, 87-93.
- Cobbold, P. Q. (1980). Development of sheath folds in shear regimes. *Journal of structural geology*.
- Carreras, J., Estrada, A., & White, S. (1977). The effects of folding on the c-axis fabrics of a quartz mylonite. *Tectonophysics*, 39(1-3), 3-24.
- Dasgupta, S., Sengupta, P., Guha, D., & Fukuoka, M. (1991). A refined garnet-biotite Fe- Mg exchange geothermometer and its application in amphibolites and granulites. *Contributions to mineralogy and petrology*, 109, 130-137.
- Deshpande, G. G., & Pitale, U. L. (2014). *Geology of Maharashtra (-Revised)*. GSI Publications, 2(1).

- Eckert, J. O., Newton, R. C., & Kleppa, O. J. (1991). The  $\Delta H$  of reaction and recalibration of garnet-pyroxene-plagioclase-quartz geobarometers in the CMAS system by solution calorimetry. *American Mineralogist*, 76(1-2), 148-160.
- Fernando O. Marques, S. M. (2008). Sheath fold development with viscosity contrast: Analogue experiments in bulk simple shear. *Journal of Structural Geology*.
- Ferry, J. T., & Spear, F. S. (1978). Experimental calibration of the partitioning of Fe and Mg between biotite and garnet. *Contributions to mineralogy and petrology*, 66(2), 113-117.
- Fossen, H. (2016). *Structural geology* (2nd ed., p. 182). Cambridge University Press.
- Fossen, H. R. (1990). Shear zone structures in the Oygarden area, west Norway. *Tectonophysics* 174.
- Foote, R. B. (2001). The geological features of the south Mahratta country and adjacent districts. *MEMOIRS-GEOLOGICAL SOCIETY OF INDIA*, (1), 43-46.
- Foote, R.B. Geological features of the south of Maharashtra and adjoining districts. 1876, *Memoir of the geological survey of india*, 12(2), 70- 133.
- Ghosh, S. K. (2004). *Structural geology* (2nd ed.). CRC Press.
- Graham, C. M., & Powell, R. (1984). A garnet–hornblende geothermometer: calibration, testing, and application to the Pelona Schist, Southern California. *Journal of metamorphic Geology*, 2(1), 13-31.
- Geological society of India, District resource map of Sindhidurg district Maharashtra 2021.
- Ghosh, S. K., S. Hazra, and S. Sengupta (1999), Planar, non-planar and refolded sheath folds in Phulad shear zone, Rajasthan, India, *J. Struct. Geol.*, 21, 1715–1729.

- Ganguly, J., & Saxena, S. K. (1984). Mixing properties of aluminosilicate garnets: constraints from natural and experimental data, and applications to geothermobarometry. *American mineralogist*, 69(1-2), 88-97.
- Ghodke, S. S. (1983). A reappraisal of stratigraphy and structure of the Dharwar supergroup of rocks of Sindhudurg district, Maharashtra. In Memorial volume in homage to Prof. KV Kelkar (pp. 15-24).
- Hobbs, B. E., Means, W. D., & Williams, P. F. (2013). *An introduction to metamorphic petrology*. Cambridge University Press.
- Hodges, K. V., & Spear, F. S. (1982). Geothermometry, geobarometry and the  $Al_2SiO_5$  triple point at Mt. Moosilauke, New Hampshire. *American mineralogist*, 67(11-12), 1118-1134.
- Holland, T., & Blundy, J. (1994). Non-ideal interactions in calcic amphiboles and their bearing on amphibole-plagioclase thermometry. *Contributions to mineralogy and petrology*, 116, 433-447.
- Hokada, T., Horie, K., Satish-Kumar, M., Ueno, Y., Nasheeth, A., Mishima, K., & Shiraishi, K. (2013). An appraisal of Archaean supracrustal sequences in Chitradurga schist belt, western Dharwar Craton, southern India. *Precambrian Research*, 227, 99-119.
- Hackler, R. T., & Wood, B. J. (1989). Experimental determination of Fe and Mg exchange between garnet and olivine and estimation of Fe-Mg mixing properties in garnet. *American Mineralogist*, 74(9-10), 994-999.
- Iyer, L. A. N. (1939). The geology of the south Ratnagiri and parts of Savantwadi state, Bombay Presidency. *Rec. Geol. Surv. India*, 74(4).
- Jacqueline E. Reber, M. D. (2013). Sheath fold morphology in simple shear. *Journal of Structural Geology*.

- Jayananda, M., Kano, T., Peucat, J. J., & Channabasappa, S. (2008). 3.35 Ga komatiite volcanism in the western Dharwar craton, southern India: Constraints from Nd isotopes and whole-rock geochemistry. *Precambrian Research*, 162(1-2), 160-179.
- Kohn, M. J., & Spear, F. S. (1989). Empirical calibration of geobarometers for the assemblage garnet+ plagioclase+ quartz. *American Mineralogist*, 74(1-2), 77-84.
- Kelly, N. M., G. L. Clarke, C. J. Carson, and R. W. White (2000), Thrusting in the lower crust: Evidence from the Oygarden Islands, Kemp Land, East Antarctica, *Geol. Mag.*, 37, 219–234.
- Martins-Ferreira, M. A. C., & Rodrigues, S. W. D. O. (2021). Field guide to RODS in the Pireneus Syntaxis, central Brazil. *Structural Geology and Tectonics Field Guidebook—Volume 1*, 221-264.
- Morimoto, N. (1988). Die Nomenklatur von Pyroxenen. *Mineralogy and Petrology*, 39, 55-76.
- Minnigh, L. (1979). Structural analysis of sheath-folds in a meta-chert from the Western Italian Alps. *Journal of Structural Geology*.
- Mishra, S. K., Pandit, M. K., & Balakrishnan, S. (2013). Geochemistry of the Sargur Group metavolcanics (Western Dharwar Craton, India) and implications for their petrogenesis and tectonic setting. *Precambrian Research*, 225, 256-274
- Molina, J. F., Moreno, J. A., Castro, A., Rodríguez, C., & Fershtater, G. B. (2015). Calcic amphibole thermobarometry in metamorphic and igneous rocks: New calibrations based on plagioclase/amphibole Al-Si partitioning and amphibole/liquid Mg partitioning. *Lithos*, 232, 286-305.
- Mandal, A., Ray, A., Debnath, M., & Paul, S. P. (2012). Petrology, geochemistry of hornblende gabbro and associated dolerite dyke of Paharpur, Puruliya, West

- Bengal: Implication for petrogenetic process and tectonic setting. *Journal of earth system science*, 121, 793-812.
- Nakamura, D. (2009). A new formulation of garnet–clinopyroxene geothermometer based on accumulation and statistical analysis of a large experimental data set. *Journal of Metamorphic Geology*, 27(7), 495-508.
- Nibir Mandal, A. K. (2009). Numerical estimation of the initial hinge-line irregularity required for the development of sheath folds: A pure shear model. *Journal of Structural Geology*.
- Naqvi, S. M., & Rogers, J. J. W. (1987). *Precambrian geology of India*.
- Nicolas, F. B. (1975). Kinematic interpretation of folds in alpine-type peridotites. *Tectonophysics*.
- Passchier, C. W., & Trouw, R. A. (2005). *Microtectonics*. Springer Science & Business Media.
- Perchuk, L. L. (1991). Derivation of a thermodynamically consistent set of geothermometers and geobarometers for metamorphic and magmatic rocks. *Progress in metamorphic and magmatic petrology*, 93-112.
- Rekha, S., & Bhattacharya, A. (2014). Paleoproterozoic/Mesoproterozoic tectonism in the northern fringe of the Western Dharwar Craton (India): its relevance to Gondwanaland and Columbia supercontinent reconstructions. *Tectonics*, 33(4), 552-580.
- Ramakrishnan, M., & Vaidyanathan, S. (2008). The Dharwar Craton (India): A review of the inferred geodynamic evolution of the ca. 3.5–2.5 Ga period, and possible implications for global tectonics. *Canadian Journal of Earth Sciences*, 45(8), 925-941

- Ramakrishnan, M., & Vaidyanadhan, R. (2010). *Geology of India* (vol. 1 & 2). GSI Publications, 2(1).
- Rao, J. R., Kumar, B. R., Balakrishna, B., & Veeraiah, B. (2021). Tectonic divisions and accretionary model within Dharwar Craton: New insights from gravity surveys on status of Chitradurga Schist Belt. *Journal of Earth System Science*, 130(3), 119.
- Ramsay, D. (1979). Analysis of rotation of folds during progressive deformation. *Geological Society of America Bulletin*
- Ramsay, J. G., & Lisle, R. J. (2000). *The techniques of modern structural geology: Volume 1. Strain analysis* (Vol. 1). Academic Press.
- Ramsay, J. G., & Huber, M. I. (1987). *Modern structural geology. Folds and Fractures*, 2, 309-700.
- Ramsay, J. G., Huber, M. I., & Lisle, R. J. (1983). *The techniques of modern structural geology: Folds and fractures* (Vol. 2). Academic press.
- Rosas, F., Marques, F. O., Luz, A., & Coelho, S. (2002). Sheath folds formed by drag induced by rotation of rigid inclusions in viscous simple shear flow: nature and experiment. *Journal of Structural Geology*, 24(1), 45-55.
- Rosenfeld, J. L., Law, R. D., Beardsmore, G. R., & Hobbs, B. E. (1998). Variation in vorticity and strain patterns in an orogenic gold deposit: a kinematic analysis of the Golden Mile, Kalgoorlie, Western Australia. *Economic Geology*, 93(2), 189-209.
- Searle, M. P., & Alsop, G. I. (2007). Eye to eye with a mega-scale sheath fold: a case study from Wadi Mayh, northern Oman Mountains. *Geology*, 35(12), 1043-1046.
- Simpson, C., & Schmid, S. M. (1983). *Principles of metamorphic deformation*. D. Reidel Publishing Company.

- Skjerna, L. (1989). Tubular folds and sheath folds definitions and conceptual models for their development, with examples from the Grapesvare Area Northern Sweden. *Journal of structural geology*.
- Spear, F. S., Kohn, M. J., Florence, F. P., & Menard, T. (1990). A model for garnet and plagioclase growth in pelitic schists: Implications for thermobarometry and P-T path determinations. *Journal of Metamorphic Geology*, 8(6), 683-696.
- SWAMI, N., & Ramakrishnan, M. (1981). HISTORICAL REVIEW OF EARLY PRECAMBRIEN SUPRACRUSTALS OF SOUTHERN KARNATAKA.
- Sreehari, L., & Toyoshima, T. (2020). Structural architecture and geological relationships in the southern part of Chitradurga Schist Belt, Dharwar craton, South India. *Journal of Mineralogical and Petrological Sciences*, 115(2), 102-117.
- Sarkar, P. K., & Soman, G. R. (1986). Geology of the area around Katta, sindhudurg district, Maharashtra. Based on aerospace data. *Journal of the Indian Society of Remote Sensing*, 14, 43-51.
- Twiss, R. J., & Moores, E. M. (1992). *Structural geology* (p. 123). W. H. Freeman and Company..
- Thompson, A. B. (1976). Mineral reactions in pelitic rocks; II, Calculation of some PTX (Fe-Mg) phase relations. *American Journal of Science*, 276(4), 425-454.
- Wilkinson C.J., (1871), Sketch of the geological structure of Southern Konkan, *Rec. Geol. Surv. India*. 6: 44–47.

